XDH-1 inactivation causes xanthine stone formation in *C. elegans* which is inhibited by SULP-4-mediated anion exchange in the excretory cell

Jennifer Snoozy[1], Sushila Bhattacharya[1], Robin R. Fettig[1,3], Ashley Van Asma, Chloe Brede[1], Kurt Warnhoff[1,2]

[1]Pediatrics and Rare Diseases Group, Sanford Research, Sioux Falls, SD 57104, USA

[2]Department of Pediatrics, Sanford School of Medicine, University of South Dakota, Sioux Falls, SD 57105 USA

[3]Department of Basic Biomedical Sciences, Sanford School of Medicine, University of South Dakota, Vermillion, SD 57069, USA

Correspondence to: Kurt Warnhoff (kurt.warnhoff@sanfordhealth.org)

Abstract:

Xanthine dehydrogenase (XDH-1) is a molybdenum cofactor (Moco) requiring enzyme that catabolizes hypoxanthine into xanthine and xanthine into uric acid, the final steps in purine catabolism. Human patients with mutations in *xdh-1* develop xanthinuria which can lead to xanthine stones in the kidney, recurrent urinary tract infections, and renal failure. Currently there are no therapies for treating human XDH-1 deficiency. Thus, understanding mechanisms that maintain purine homeostasis is an important goal of human health. Here, we used the nematode *C. elegans* to model human XDH-1 deficiency using 2 clinically relevant paradigms, Moco deficiency or loss-of-function mutations in *xdh-1.* Both Moco deficiency and *xdh-1* mutations caused the formation of autofluorescent xanthine stones in *C. elegans*. Surprisingly, only 2% of *xdh-1* null mutant *C. elegans* developed a xanthine stone, suggesting additional pathways may regulate this process. To uncover such pathways, we performed a forward genetic screen for mutations that enhance the penetrance of xanthine stone formation in *xdh-1* null mutant *C. elegans*. We isolated multiple loss-of-function mutations in the gene *sulp-4* which encodes a transmembrane transport protein homologous to human SLC26 anion exchange proteins. We demonstrated that SULP-4 acts cell-nonautonomously in the excretory cell to limit xanthine stone accumulation. Interestingly, *sulp-4* mutant phenotypes were suppressed by mutations in genes that encode for cystathionase (*cth-2)* or cysteine dioxygenase (*cdo-1*), members of the sulfur amino acid metabolism pathway required for production of the osmolyte taurine. Furthermore, *cdo-1* mRNA accumulated in *sulp-4* mutant animals, mirroring *cdo-1* activation observed during hyperosmotic stress in *C. elegans* and mammals. We propose that loss of SULP-4-mediated anion exchange causes osmotic stress and *cdo-1* activation, a maladaptive response that promotes xanthine stone accumulation. Supporting the model that the osmotic stress response impacts xanthine stone accumulation, a mutation in *osm-8* that constitutively activates the osmotic stress response, also promoted xanthine stone accumulation in an *xdh-1* mutant background. Thus, our work establishes a *C. elegans* model for human XDH-1 deficiency and identifies *sulp-4* and the osmotic stress response governed by *cdo-1* as critical players in controlling xanthine stone accumulation.

Background:

Purines are an abundant and fundamental metabolite class that are essential for the generation of RNA and DNA molecules while purine nucleotides are critical energy sources (ATP) and signaling molecules (GTP). Failures in purine metabolism can lead to both common and rare diseases. For instance, oncogenic mutations activate nucleotide biosynthetic capacity in diverse cancers, promoting cancer progression [1]. Mutations in enzymes in the purine metabolic pathway cause rare inborn errors of metabolism such as Lesch-Nyhan syndrome, purine nucleoside phosphorylase deficiency, and xanthinuria [2-5]. Thus, understanding the mechanisms that impact purine homeostasis is an important goal of human health.

Xanthinuria, an inborn error of purine metabolism, is caused by inactivation of xanthine dehydrogenase (XDH), the terminal enzyme in purine catabolism that oxidizes hypoxanthine to xanthine and xanthine to uric acid [6] (**Fig. 1A**). There are two types of human xanthinuria; type I is caused by mutations in the gene encoding the xanthine dehydrogenase enzyme and type II is caused by mutations in enzymes that synthesize the molybdenum cofactor (Moco), an essential prosthetic group for XDH [4, 5]. Both forms of xanthinuria present with high levels of xanthine in the urine and low levels of uric acid which can result in the formation of xanthine stones in kidneys and muscles, sometimes causing renal failure. There is currently no curative therapy for xanthinuria, however high fluid intake and low purine diets are recommended for patients [7].

XDH requires Moco for its enzymatic function. Moco is a prosthetic group that is required for development in animals ranging from the nematode *C. elegans* to humans [4, 8]. Moco is synthesized by an ancient and conserved biosynthetic pathway [9]. *C. elegans* has recently emerged as a powerful model system for studying Moco biology, and the genes that encode the Moco biosynthetic pathway are termed *moc* in *C. elegans* for MOlybdenum Cofactor biosynthesis [8, 10]. In addition to endogenous Moco synthesis, *C. elegans* can also acquire and use Moco from its bacterial diet [8, 11, 12]. Given its genetic tractability and the ability to manipulate animal Moco content by simple dietary manipulation, *C. elegans* is a useful model for understanding the biology of Moco and Moco-requiring enzymes, such as XDH.

Here, we genetically explored the formation of xanthine stones in *C. elegans,* which emerge during Moco deficiency or in *xdh-1* mutant *C. elegans,* mirroring type I and type II human xanthinuria [4, 5]. Surprisingly, only a small percentage of Moco-deficient and *xdh-1* mutant *C. elegans* developed xanthine stones, suggesting additional parallel pathways for maintaining purine homeostasis. To identify novel regulators of xanthine stone accumulation, we performed an unbiased chemical mutagenesis screen for mutations that enhanced the penetrance of xanthine stone formation in *xdh-1* mutant animals. In this screen we recovered five loss-of-function alleles of *sulp-4,* a gene which encodes a member of the sulfate permease family of transporters with homology to human SLC26 transporters [13]. We demonstrated that SULP-4 acts in the *C. elegans* excretory cell, analogous to the human kidney, to inhibit the accumulation of xanthine stones [14]. We further showed that *sulp-4* was required for normal development. Interestingly, we found that phenotypes caused by *sulp-4* loss of function were suppressed by inactivating mutations in

cth-2 or *cdo-1,* genes that encode core members of the sulfur amino acid metabolism pathway required for synthesis of the osmolyte taurine [8]. We suggest that *sulp-4* loss of function promotes xanthine stone accumulation because of disrupted osmotic homeostasis. This model is supported by the observation that mutations in *osm-8* that constitutively activate the osmotic stress response, also promote xanthine stone accumulation in an *xdh-1* mutant background. Thus, our work establishes a *C. elegans* model for the rare genetic disease xanthinuria and identifies *sulp-4* as a potent genetic modifier of this disease pathology in *C. elegans,* likely acting through disrupted osmotic homeostasis.

Results:

XDH-1 inactivation caused the accumulation of xanthine stones in *C. elegans*.

To explore the pathology of Moco deficiency in the nematode *C. elegans,* we cultured *cth-2; moc-1* and *moc-1 cdo-1* double mutant animals on wild type (Moco replete) or *ΔmoaA* mutant (Moco deficient) *E. coli*. The *moc-1* mutation prevents the endogenous synthesis of Moco while the *cth-2* and *cdo-1* mutations suppress the lethality typically associated with animal Moco deficiency [8]. Thus, by changing the dietary *E. coli*, we can control whether the animals have Moco. When culturing *cth-2; moc-1* double mutant animals on Moco- *E. coli* we surprisingly observed animals that developed autofluorescent stones, typically found in the posterior of the intestine. 54% of *cth-2; moc-1* animals fed a Moco- diet developed an autofluorescent stone while 0% of *cth-2; moc-1* animals developed an autofluorescent stone when fed a diet that provided Moco. We observed similar results for *moc-1 cdo-1* double mutant animals where 17% of animals developed an autofluorescent stone on Moco- *E. coli* and 0% developed a stone when fed wild-type *E. coli* (**Fig. 1B**). Thus, we conclude that the formation of these autofluorescent stones is caused by Moco deficiency.

Surprisingly, we also observed the formation of autofluorescent stones in 8% of wild-type *C. elegans* when cultured on Moco- *E. coli.* 0% of wild-type animals developed an autofluorescent stone when fed Moco+ *E. coli* (**Fig. 1B**). This result demonstrates that dietary Moco deficiency alone is sufficient to promote the formation of autofluorescent stones. This result is surprising as wild-type animals are still competent to produce Moco through their endogenous biosynthetic pathway. However, these data are consistent with our recent findings that the *C. elegans* diet plays a significant role in promoting Moco homeostasis [12].

Given that the development of these autofluorescent stones was dependent upon dietary Moco deficiency, we reasoned that the phenotype was likely being caused by inactivation of one of the four animal Moco-requiring enzymes. Interestingly, inactivation of the Moco-requiring enzyme xanthine dehydrogenase causes the accumulation of insoluble and fluorescent xanthine stones in organisms as diverse as plants, fruit flies, and humans [5, 15-19]. We therefore hypothesized that the autofluorescent stones we observed during *C. elegans* Moco deficiency were xanthine stones. To test this, we looked for the presence of autofluorescent stones in animals carrying the *ok3234* null mutation in *xdh-1,* the *C. elegans* orthologue of xanthine dehydrogenase. When we cultured *xdh-1* null mutant *C. elegans* on wild-

type *E. coli* we indeed observed the formation of highly autofluorescent stones in 2% of animals (**Fig. 1B,C**). Thus, *xdh-1* was necessary for inhibiting the formation of autofluorescent stones. Consistent with their presence in diverse models of XDH-1-deficiency, we propose that the autofluorescent stones we observe during Moco- and XDH-1- deficiency in *C. elegans* are xanthine stones.

sulp-4 inhibited the formation of xanthine stones.

XDH-1 functions at the end of the purine catabolism pathway to oxidize hypoxanthine to xanthine and xanthine to uric acid (**Fig. 1A**). Given the critical position of XDH-1 in purine metabolism, we were surprised that only 2% of *xdh-1* null mutant animals developed a xanthine stone. This result suggests the existence of parallel pathways for maintaining purine homeostasis. To identify additional regulators of purine metabolism, we performed an unbiased chemical mutagenesis screen for mutations that enhanced the penetrance of the xanthine stone phenotype. We mutagenized *xdh-1* mutant *C. elegans* with ethyl methanesulfonate (EMS) and cultured the newly mutagenized animals for 2 generations allowing newly induced mutations to become homozygous [20]. We then cloned single mutagenized F2 animals onto their own petri dish and screened for clones where we observed a high fraction of F3 progeny developing xanthine stones.

Here we describe five new EMS-induced recessive loss-of-function mutations that caused a high penetrance of xanthine stone formation in an *xdh-1* mutant background, *rae299, rae302, rae319, rae320* and *rae326* (**see Methods**). These mutant alleles were prioritized because they displayed strong enhancement of xanthine stone formation and formed a complementation group, indicating they affect a single gene (**see Methods**). To identify the causative genetic lesions in these new mutant strains, genomic DNA from all five strains was analyzed via whole genome sequencing. Our complementation studies suggested that the mutant strains should have novel mutations in a common gene. Only one gene, *sulp-4,* was uniquely mutated in all five strains, strongly suggesting these mutations were causative for the enhanced penetrance of xanthine stone formation in the *xdh-1* mutant animals (**Fig. 2A,B, Table S1**). Among the newly isolated *sulp-4* alleles we found 3 missense and 2 splice site mutations. Based on their recessive nature and molecular identities, we propose that these are loss-of-function alleles of *sulp-4.*

To test the hypothesis that loss of *sulp-4* function causes enhanced xanthine stone accumulation in an *xdh-1* mutant, we used CRISPR/Cas9 to engineer a new *sulp-4* deletion allele, *rae334* [21, 22]. The *sulp-4(rae334)* allele is a 683 bp deletion that eliminates part of exon 1, all of exons 2 and 3, and part of exon 4 (**Fig. 2A**). Thus, we propose that *sulp-4(rae334)* encodes a null allele. The *sulp-4(rae334)* allele strongly enhanced the penetrance of xanthine stone formation in *xdh-1* mutant *C. elegans,* phenocopying the *sulp-4* alleles isolated in our EMS screen (**Fig. 2B**). These data demonstrate that the *sulp-4* lesions identified by whole genome sequencing cause xanthine stone accumulation in *xdh-1* mutant animals. Furthermore, these data show that *sulp-4* acts in parallel with *xdh-1* to inhibit the accumulation of xanthine stones.

The xanthine stones observed in *xdh-1; sulp-4* double mutant animals localized to the posterior of the *C. elegans* intestinal lumen, consistent with the localization of the stones observed in *xdh-1* mutant

animals (**Fig. 2C**)**.** In addition to observing xanthine stones at a higher frequency in *xdh-1; sulp-4* mutant animals, the xanthine stones were also much larger suggesting that *sulp-4* loss of function enhances both the penetrance and expressivity of the xanthine stone phenotype in *xdh-1* mutant animals (**Fig. S1**).

We originally observed the formation of xanthine stones during conditions of Moco deficiency; *cth-2; moc-1* double mutant animals feeding on Moco- *E. coli.* We hypothesized that the *sulp-4* mutation would also enhance the formation of xanthine stones caused by Moco deficiency. To test this, we assayed xanthine stone formation in *sulp-4* single mutant animals cultured on wild-type or Moco- *E. coli*. 89% of *sulp-4* mutant animals developed xanthine stones during dietary Moco deficiency compared to 1% of *sulp-4* mutant animals fed a Moco replete diet (**Fig. S2A**). These data are consistent with our conclusion that *sulp-4* functions to limit the accumulation of xanthine stones caused by XDH-1 inactivation resulting from either Moco insufficiency or an *xdh-1* mutation.

***sulp-4* promoted healthy larval and embryonic development.**

While culturing the *sulp-4(rae334)* mutant strain, we observed that mutant animals were sick and slow growing. Thus, we explored the role of *sulp-4* in development and embryonic viability. To test the impact of *sulp-4* loss of function on developmental rate, we synchronized wild-type, *sulp-4(rae319),* and *sulp-4(rae334)* animals at the first stage of larval development and assayed their growth after 72 hours. We found that *sulp-4(rae334)* animals displayed a severe developmental delay compared to the wild type (**Fig. 2D**). Interestingly, *sulp-4(rae319)* animals showed a more subtle developmental delay. Thus, we propose that *sulp-4(rae334)* is a null allele while *sulp-4(rae319)* represents a hypomorph. Similarly, we observed that *sulp-4(rae334)* caused 18% embryonic lethality while *sulp-4(rae319)* caused 5% embryonic lethality. No embryonic lethality was observed for wild-type *C. elegans* (**Fig. 2E**). Thus, we conclude that *rae334* and *rae319* represent an allelic series for *sulp-4* and that *sulp-4* is necessary for promoting embryonic and larval development in *C. elegans.*

***pnp-1* was necessary for the formation of xanthine stones in *xdh-1; sulp-4* mutants but dispensable for the developmental delay caused by *sulp-4* loss of function.**

To further test the model that the autofluorescent stones observed in *xdh-1; sulp-4* mutant animals were composed of xanthine, we performed genetic epistasis with a null mutation in purine nucleoside phosphorylase (*pnp-1*), a gene necessary for the formation of hypoxanthine and xanthine (**Fig. 1A**) [23]. As previously observed, *xdh-1; sulp-4* double mutant animals displayed 98% autofluorescent stone formation while *pnp-1 xdh-1; sulp-4* triple mutant *C. elegans* displayed 3% formation of autofluorescent stones (**Fig. 3A**). Thus, *pnp-1* was necessary for the formation of the autofluorescent stones observed in *xdh-1; sulp-4* double mutants. Given that *pnp-1* plays a conserved role in the formation of hypoxanthine and xanthine, these results support our model that the autofluorescent stones we observe are likely to be predominantly composed of xanthine. Although, we cannot exclude the possibility that other metabolites, such as hypoxanthine, are also present in the autofluorescent stones.

To determine if *pnp-1* acts in a genetic pathway with *sulp-4,* we tested the impact of *pnp-1* loss of function on the developmental delay displayed by *sulp-4* mutant animals. *pnp-1; sulp-4* double mutant

larvae developed at a rate similar to *sulp-4* single mutant animals. Importantly, *pnp-1* mutant animals displayed healthy larval development (**Fig. 3B**). Thus, *pnp-1* was not required for the developmental delay displayed by *sulp-4* mutant *C. elegans.* We propose a genetic pathway where *pnp-1* promotes the formation of xanthine stones epistatic to the function of *xdh-1* and in parallel to the activity of *sulp-4*.

sulp-4/SLC26 encodes an anion exchange protein that acted in the excretory cell to promote xanthine homeostasis.

sulp-4 encodes a transmembrane transporter with homology to the SLC26 family of anion transporters in mammals [13, 24]. The *C. elegans* genome encodes eight members of the SLC26 transporter family, named SULP-1 through SULP-8 [13]. We wondered if other members of the SLC26 family of transporters also played a role in limiting the formation of xanthine stones. To test this, we cultured viable strains with deletions in *sulp-1, sulp-2, sulp-4, sulp-5, sulp-7,* and *sulp-8* on Moco- *E. coli* and assayed the formation of xanthine stones. Only the strain carrying the *sulp-4* mutation displayed a high penetrance of xanthine stones (79%, **Fig. S2B**). Thus, the enhancement of xanthine stone formation is specific to loss of *sulp-4* and not a general feature of *sulp* inactivation.

SULP-4 is expressed in the apical membrane of the *C. elegans* excretory cell, a single cell that plays roles in ionic regulation and waste elimination analogous to the mammalian renal system [13, 14, 25]. Studies of SULP-4 expressed in *Xenopus* oocytes demonstrate that SULP-4 is sufficient to promote the transport of sulfate and, to a lesser extent, chloride [13]. To determine the site of action of *sulp-4* with respect to the xanthine stone formation phenotype, we generated transgenic *xdh-1; sulp-4* double mutant *C. elegans* expressing a *Psulp-4::SULP-4::GFP* translational fusion transgene (plasmid was a gift from Dr. Keith Nerhke) [13]. Consistent with previous reports, we exclusively saw expression of the *Psulp-4::SULP-4::GFP* translational fusion in the excretory cell (**Fig. 4A,B**). To test the functionality of the *Psulp-4::SULP-4::GFP* transgene, we performed rescue experiments by generating *xdh-1; sulp-4* double mutant animals expressing *Psulp-4::SULP-4::GFP* and assaying the formation of xanthine stones. *xdh-1; sulp-4* double mutant animals expressing the *Psulp-4::SULP-4::GFP* did not develop xanthine stones, demonstrating functional transgenic rescue. This rescue was observed in three independently derived transgenic strains (**Fig. 4C**). Thus, the *Psulp-4::SULP-4::GFP* transgenic fusion protein was functional, suggesting that its expression pattern faithfully represents endogenous SULP-4 localization. We conclude that SULP-4 acts in the excretory cell to negatively regulate the formation of xanthine stones. Our observation that *xdh-1; sulp-4* double mutant animals typically develop xanthine stones in the intestinal lumen suggests that *sulp-4* is functioning cell non-autonomously to limit the formation of xanthine stones.

To further test the role of the excretory cell in preventing the formation of xanthine stones, we used an *exc-5* mutation that causes defects in excretory cell development and morphology [26]. We reasoned a malformed excretory cell may not function efficiently and thus phenocopy *sulp-4* loss of function with respect to xanthine stone formation. Indeed, *exc-5; xdh-1* double mutant animals displayed enhanced formation of xanthine stones (**Fig. S3A**)**.** Although, the xanthine stone penetrance of the *exc-5; xdh-1* (16%) double mutant strain was modest compared to *xdh-1; sulp-4*. Importantly, *sulp-4* loss of function did

not cause defects in excretory cell morphology (**Fig. S3B-D**). We conclude that the enhancement of xanthine stone formation caused by inactivating mutations in *sulp-4* result from loss of SULP-4 anion exchange function and not broader defects in excretory cell biology.

***cth-2* and *cdo-1* were necessary for *sulp-4* mutant phenotypes.**

sulp-4 inactivation caused xanthine stone formation during dietary Moco deficiency (**Fig. S2A, Fig. S4A**), demonstrating that the enhancement of xanthine stones caused by *sulp-4* loss of function occurs even when endogenous Moco biosynthesis is functional. To test the impact of a *sulp-4* mutation on xanthine stone formation during complete Moco deficiency, we engineered *sulp-4; cdo-1 moc-1* triple mutant *C. elegans* that cannot synthesize their own Moco (caused by *moc-1* mutation) and are viable during Moco deficiency (caused by *cdo-1* suppressor mutation) (**Fig. 5A**). When cultured on Moco- *E. coli, sulp-4; cdo-1 moc-1* triple mutants are completely Moco deficient yet only displayed 9% penetrance of xanthine stones (**Fig. S4A**). Similarly, *sulp-4; cdo-1* double mutant animals cultured on Moco- *E. coli* displayed 0% penetrance of xanthine stones, dramatically reduced compared to the 85% penetrance displayed by *sulp-4* mutants cultured on Moco- *E. coli* (**Fig. S4A**). These results were surprising and suggest that *cdo-1* is necessary for the formation of xanthine stones caused by a *sulp-4* mutation and Moco deficiency.

To further test the impact of *cdo-1* on the formation of xanthine stones, we engineered *xdh-1; sulp-4; cdo-1* triple mutants. Surprisingly, *xdh-1; sulp-4; cdo-1* triple mutants displayed a 4% xanthine stone penetrance, dramatically reduced when compared to the 98% penetrance displayed by *xdh-1; sulp-4* double mutant animals (**Fig. 5B**). Thus, *cdo-1* was necessary for the formation of xanthine stones displayed by *xdh-1; sulp-4* double mutants. Interestingly, we still observe a low penetrance of xanthine stones in *xdh-1; sulp-4; cdo-1* triple mutants suggesting that *cdo-1* activity is not absolutely required for the formation of xanthine stones but only required for the xanthine stone enhancement caused by *sulp-4* loss of function.

cdo-1 encodes the *C. elegans* cysteine dioxygenase, a critical enzyme in the in sulfur amino acid catabolism pathway that breaks down excess cysteine and methionine and is essential for synthesis of the osmolyte taurine (**Fig. 5A**) [8, 27, 28]. To determine if the impact of *cdo-1* on the enhanced xanthine stone formation caused by *sulp-4* inactivation was a result of impaired sulfur amino acid catabolism, we used a *cth-2* mutation which eliminates the activity of *C. elegans* cystathionase (**Fig. 5A**). Consistent with our results with *cdo-1* loss of function, we found that *cth-2; xdh-1; sulp-4* triple mutant animals also displayed a low 19% penetrance of xanthine stones (**Fig. 5B**). Taken together, these genetic data suggest that sulfur amino acid catabolism is required for the enhancement of xanthine stone accumulation caused by loss of *sulp-4* function.

To test whether mutations in *cth-2* or *cdo-1* would suppress the defects in larval and embryonic development displayed by *sulp-4* mutant animals, we assayed larval and embryonic development in *cth-2; sulp-4* and *sulp-4; cdo-1* double mutant animals and compared to *sulp-4* single mutant animals. Consistent with their suppression of xanthine stone formation, *cth-2* or *cdo-1* mutations suppressed the

developmental delay and embryonic lethality caused by a *sulp-4* mutation (**Fig. 5C,D**). Thus, we conclude that *cth-2* and *cdo-1* are broadly required for phenotypes caused by *sulp-4* loss of function (**Fig. 5E**).

Loss of *osm-8* promoted xanthine stone accumulation in *xdh-1* mutant animals, linking the osmotic stress response and xanthine stone formation.

What is the physiological intersection between *sulp-4* and the sulfur amino acid catabolism pathway governed by *cth-2* and *cdo-1*? Given that *sulp-4* encodes an anion exchange protein that functions in the *C. elegans* excretory cell, we hypothesized that *sulp-4* mutant animals may be experiencing osmotic stress even when cultured under normal laboratory growth conditions. To maintain osmotic homeostasis, cellular concentrations of non-ionic osmolytes such as taurine, glycerol, and *myo*-inositol are dramatically increased through activation of osmolyte synthesis or import. This adaptive response normally functions to osmotically equilibrate cells with their environment without dramatically altering ionic composition of the cell.

To test the model that *sulp-4* loss of function is causing osmotic stress, we examined the transcription of three genes that are critical for promoting osmolyte accumulation: *cdo-1, gpdh-1,* and *hmit-1.1.* As discussed above, *cdo-1* encodes cysteine dioxygenase, an enzyme that is required to produce the osmolyte taurine [28, 29]. *gpdh-1* encodes glycerol 3-phosphate dehydrogenase and is required to produce glycerol, a critical osmolyte [30, 31]. Finally, *hmit-1.1* encodes an H^+/*myo*-inositol transporter and functions to import *myo*-inositol, another important osmolyte [32]. All three of these genes are transcriptionally induced via hyperosmotic stress and by genetic lesions such as *osm-8(n1518)* that activate the hyperosmotic stress response [33]. Using qPCR, we observed that *cdo-1* mRNA was consistently elevated in both *sulp-4* (~8-fold) and *osm-8* (~4-fold) mutant animals compared to the wild type **(Fig. 6A**). Similarly, *gpdh-1* and *hmit-1.1* mRNA also appeared to be mis-regulated in *sulp-4* mutant animals. However, these results showed high variability and were not consistently reproducible when RNA was isolated from either the *sulp-4* or *osm-8* mutant animals (**Fig. S4C,D**). These results were unexpected given the established role of *osm-8* in the transcriptional regulation of *hmit-1.1* and *gpdh-1* [33, 34]. We suspect our rigorous washing of *C. elegans* samples prior to RNA isolation may impact the osmotic environment of our animals, muting the established transcriptional activation of *hmit-1.1* and *gpdh-1* (**see Methods)**. Nevertheless, our data demonstrate that *cdo-1* mRNA accumulates during *sulp-4* or *osm-8* inactivation. Thus, we propose that *sulp-4* mutant *C. elegans* may be experiencing hyperosmotic stress.

Given that *cdo-1* was necessary for phenotypes caused by *sulp-4* inactivation, we wondered whether inactivating mutations in other osmotic response genes may also suppress *sulp-4* mutant phenotypes. To test this, we engineered *gpdh-1; sulp-4* and *hmit-1.1; sulp-4* double mutant strains of *C. elegans* and assayed for the formation of xanthine stones when animals were cultured on a Moco- diet. Unlike *cdo-1,* neither *gpdh-1* nor *hmit-1.1* were necessary for the formation of xanthine stones caused by a *sulp-4* mutation (**Fig. S4B**). These data suggest that the suppression *sulp-4* mutant phenotypes by *cdo-1* loss-of-function is specific and not a general feature of inactivating mutations in genes involved in the osmotic stress response.

To determine if activating the hyperosmotic stress response is sufficient to promote xanthine stones in an *xdh-1* mutant background, we used a loss-of-function mutation in *osm-8* that constitutively activates the hyperosmotic stress response in the absence of environmental osmotic stress [33, 34]. Interestingly, *osm-8; xdh-1* double mutant *C. elegans* developed xanthine stones like *xdh-1; sulp-4* double mutant animals (**Fig. 6B)**. Although, the xanthine stones observed in *osm-8; xdh-1* double mutant animals were not as large as those observed in *xdh-1; sulp-4* animals (**Fig. S1).** Furthermore, like *xdh-1; sulp-4* double mutants, *cdo-1* was necessary for the formation of xanthine stones in the *osm-8; xdh-1* double mutant animals, implying a common genetic pathway controlling xanthine stone formation downstream of *osm-8* and *sulp-4* mutations (**Fig. 6B)**. However, it should be noted that *cdo-1* loss of function only partially suppressed the formation xanthine stones in *osm-8; xdh-1* mutant animals. This suggests there may be additional factors downstream of *osm-8* governing xanthine homeostasis. Taken together, these data suggest that proper osmotic regulation is critical to prevent the formation of xanthine stones when *xdh-1* activity is limited.

Discussion:

Modeling xanthinuria in C. elegans.

Human xanthinuria was originally described in 1954, and presents with high urinary xanthine, low uric acid in serum and urine, the formation of xanthine stones, and, in some cases, renal failure [5]. Still, there are no curative treatments for xanthinuria or the formation of xanthine stones. The current recommendation for patients is a high fluid intake and low purine diet [7]. Thus, understanding the cellular mechanisms that regulate the pathology associated with xanthinuria is an important goal.

Animal models, such as *C. elegans,* have proven to be powerful tools for exploring the pathology of rare inborn errors of metabolism including NGLY1 deficiency, Moco deficiency, Friedrich's ataxia, and many others [8, 35, 36]. Here we use *C. elegans* to model human type I and type II xanthinuria. We employed genetic strategies to inhibit XDH-1 activity by mutating the *xdh-1* gene (type I) or limiting animal Moco (type II) [4, 5]. Both manipulations recapitulate a critical feature of human XDH deficiency, the formation of insoluble xanthine stones.

Interestingly, xanthine stones are highly autofluorescent and visible with a standard fluorescence microscope, a phenotype that has been previously characterized in the model plant *Arabidopsis thaliana* [17]. Given the transparent nature of *C. elegans,* this phenotype empowers genetic analyses of xanthine stone accumulation and, by proxy, purine biology. Here we use the power of *C. elegans* genetics in combination with this simple phenotype to identify and characterize regulators of purine homeostasis.

Defining genetic regulators of xanthine stone formation.

We sought to define genetic regulators of the formation of xanthine stones. Given the established purine catabolism pathway (**Fig. 1A)**, we used a hypothesis-driven approach to define genes that regulate the formation of xanthine stones. Purine nucleoside phosphorylase (PNP-1/PNP) was a lead candidate given its biochemical requirement for the formation of xanthine. Indeed, we demonstrated that *pnp-1* was

necessary for the formation of xanthine stones in our *C. elegans* mutant animals. While *pnp-1* loss of function suppressed the formation of xanthine stones in an *xdh-1; sulp-4* double mutant background, it did not suppress the developmental phenotypes caused by *sulp-4* loss of function. These results suggest that *pnp-1* is not acting downstream of *sulp-4* to control development and is consistent with the established role of PNP-1 acting in the purine catabolism pathway with XDH-1 (**Fig. 5E)**. These results suggest that inhibiting the activity of purine nucleoside phosphorylase may be a therapeutic strategy for limiting the accumulation of xanthine and xanthine stones in patients suffering from xanthinuria. However, this treatment strategy may be fraught, given the consequences of PNP inactivation. Human patients with purine nucleoside phosphorylase deficiency display impaired T-cell immunity [3]. In fact, a potent PNP inhibitor has been developed, and induces apoptosis of B- and T-lymphocytes [37, 38]. Thus, the potential benefits of PNP inhibition in the treatment of human xanthinuria patients would need to be evaluated and weighed against the negative impacts on the immune system.

To identify new and unexpected regulators of purine homeostasis, we employed an unbiased genetic approach. In a forward genetic screen, we identified *sulp-4* as a potent modifier of xanthine stone formation. Loss-of-function mutations in *sulp-4* dramatically enhanced the penetrance and expressivity of xanthine stone formation in our *C. elegans* model of xanthinuria. These genetic data demonstrate that *sulp-4* normally acts to limit the formation of xanthine stones. Interestingly, we also found that *sulp-4* was necessary for promoting normal larval and embryonic development, as *sulp-4* mutant animals displayed delayed larval development and embryonic hatching defects. *sulp-4* encodes a transmembrane transport protein homologous to human SLC26A5/6 which function in Cl^-/HCO_3 exchange and oxalate secretion in the kidney in addition to secretion of oxalate from the small intestine [39, 40]. Heterologous transport assays of *C. elegans* SULP-4 expressed in *Xenopus* oocyes demonstrate that chloride and sulfate are transported by SULP-4 [13]. Thus, we propose that failures in the transport of these, and potentially other, anions cause the increased xanthine stone accumulation and developmental defects observed in *sulp-4* mutant animals.

SULP-4 was previously demonstrated to localize to the apical membrane of the excretory cell, which we also observed [13]. Importantly, we demonstrate that *Psulp-4::SULP-4::GFP* rescues the formation of xanthine stones displayed by an *xdh-1; sulp-4* double mutant animal. This functional rescue is strong evidence that *sulp-4* is acting in the excretory cell to limit the formation of xanthine stones. Interestingly, xanthine stones accumulate in the lumen of the *C. elegans* intestine while *sulp-4* acts in the excretory cell. Thus, we conclude that *sulp-4* acts cell-nonautonomously to limit xanthine stone accumulation. These data establish a new intersection between SULP-4, the excretory cell, and purine homeostasis.

SULP-4 homologues are implicated in calcium oxalate stone formation.

Kidney stones, the formation of solid masses of salts, minerals, or metabolites in the urinary tract, are an important health concern. About 1 out of every 10 individuals in the United States will develop a kidney stone over the course of their lifetimes [41]. Kidney stones are not uniform, and are diverse in

composition, frequency, and pathophysiology [42]. For example, calcium oxalate stones account for about half of all reported kidney stones while xanthine stones are exceedingly rare [5].

Our genetic studies demonstrate that the SLC26 family member, SULP-4, plays a role in mediating the formation of xanthine stones in *C. elegans.* Interestingly, we are not the first to report a role for SLC26 family members in metabolic stone formation. Mouse SLC26A6 has been shown to limit urolithiasis, paralleling our results with *C. elegans* SULP-4. Specifically, SLC26A6 null mutant mice develop a high incidence of calcium oxalate stones in the bladder [43]. Similarly, a dominant negative mutation in SLC26A6 and loss of function mutations in SLC26A1 are proposed to cause calcium oxalate nephrolithiasis in humans [44, 45]. In contrast, the *Drosophila melanogaster* homolog of human SLC26A5/6, dPrestin, promotes the formation of calcium oxalate stones in the Malpighian tubules in a dietarily-induced model of calcium oxalate nephrolithiasis. Under a diet of high oxalate, *Drosophila* develop calcium oxalate stones whose formation is dampened by RNAi knockdown of dPrestin [46]. With respect to calcium oxalate stones, the mechanism of stone formation is believed to relate directly to the role of the SLC26 family members in oxalate transport. Loss of SLC26 proteins results in higher or lower concentrations of oxalate in a given space, altering the likelihood of stone formation. In contrast, we propose that xanthine is the critical component of the stones that form in *xdh-1; sulp-4* mutant animals, not oxalate. In heterologous transport assays, oxalate was not meaningfully transported by SULP-4 [13]. However, it is possible that *sulp-4* mutations may enhance the formation of additional metabolic stones given a specific genetic or environmental perturbation. This hypothesis remains to be tested. Regardless, we think it is very intriguing that SLC26 homologues in mouse, humans, flies, and worms have all been shown to play roles in metabolic stone formation and suggests the potential for a fundamental mechanism underlying these discrete observations.

Implications for the osmotic stress response in the formation of xanthine stones.

We next sought to understand the molecular nature of the genetic interaction between *sulp-4* and *xdh-1* with respect to xanthine stone formation. Given that *sulp-4* encodes an anion exchange protein that transports chloride and sulfate ions and acts cell-nonautonomously in the excretory cell, we hypothesized that *sulp-4* mutations may disturb osmotic balance in *C. elegans* [13]. We imagined that disturbed osmoregulation may cause higher solute concentrations in a given fluid (such as the lumen of the *C. elegans* intestine) and result in an increased likelihood of stone formation. Disturbances in water homeostasis are known to contribute to stone formation, as dehydration is a key risk factor for human kidney stones [47]. Several lines of evidence support our model that *sulp-4* loss of function is causing disturbed osmotic homeostasis which in turn promotes xanthine stone formation: i) *sulp-4* mutants induced the transcription of *cdo-1,* a gene that is also induced by a high salt diet in both *C. elegans* and mammals [29, 33]. Furthermore, it appears that *sulp-4* loss of function also altered the expression of *gpdh-1* and *hmit-1.1,* additional genes involved in the response to high salt stress [33, 34]. Although, it is important to note that our data supporting this claim are inconsistent and not statistically significant. ii) Activation of the high salt response through a distinct genetic perturbation, *osm-8* loss of function*,* also promoted the

formation of xanthine stones in an *xdh-1* mutant background [34]. iii) Finally, inactivation of CDO-1 which is required for the production of the osmolyte taurine [28], suppressed the enhanced formation of xanthine stones caused by both *osm-8* and *sulp-4* loss of function mutations. Together, these results support the model that, in an *xdh-1* mutant background, activation of the osmotic stress response, and specifically *cdo-1,* is maladaptive and promotes the formation of xanthine stones. While a role for water homeostasis has long been appreciated in the control of kidney stone formation and treatment, our studies uncover a new genetic pathway that regulates these phenomena in a whole animal system and may offer new therapeutic targets for the treatment of urinary stone disease.

Intersection between sulfur amino acid metabolism and Moco-dependent metabolism.

Previous studies in *C. elegans* identified *cth-2* and *cdo-1* loss of function mutations as suppressors of the lethality associated with Moco deficiency and deficiency of the Moco-requiring enzyme sulfite oxidase [8]. Loss of sulfite oxidase is lethal in *C. elegans* and humans due to the accumulation of its reactive and toxic substrate, sulfite [8, 48]. *cth-2* and *cdo-1* inactivation limit the accumulation of sulfites, suppressing the lethality caused by Moco or sulfite oxidase deficiency. Is it a coincidence that loss of *cth-2* or *cdo-1* suppress phenotypes associated with two distinct Moco-requiring enzymes, i) lethality displayed by *suox-1* null mutant animals and ii) xanthine stone formation of *xdh-1; sulp-4* double mutant animals? Given that the substrates and products of these two Moco-dependent enzymes are distinct, it is peculiar that loss-of-function phenotypes of both are modulated by these common genetic factors. Future studies are required to tease apart the potential molecular intersections between CTH-2/CDO-1 and these Moco-dependent pathways.

An additional layer of complexity is added when considering the regulation of *cdo-1.* Here, we reinforce previous observations that *cdo-1* is activated in response to hyperosmotic stress [29, 33]. *sulp-4* and *osm-8* mutant *C. elegans* both accumulated *cdo-1* mRNA. Yet, CDO-1/CDO1 levels and activity are also modified by dietary sulfur amino acid content. This regulation includes both transcriptional and post-translational control of cysteine dioxygenase [27, 49-53]. Given that SULP-4 has been shown to mediate sulfate transport and sulfate is a metabolic product of sulfur amino acid metabolism governed by CTH-2/CDO-1/SUOX-1, sulfate seems like a potential metabolic intersection between these seemingly disparate Moco-dependent pathways. Whether there is any overlap between the mechanisms of CDO-1/CDO1 regulation downstream of hyperosmotic stress and high sulfur amino acid content remains to be studied.

Materials and methods:

General methods and strains:

C. elegans were cultured using established protocols [20]. Briefly, animals were cultured at 20°C on nematode growth media (NGM) seeded with wild-type *E. coli* (OP50) unless otherwise noted. The wild-type strain of *C. elegans* was Bristol N2. Additional *E. coli* strains used in this work were BW25113 (Wild type, Moco+) and JW0764-2 (Δ*moaA753::kan,* Moco-) [54].

C. elegans mutant and transgenic strains used in this work are listed here. When previously published, sources of strains are referenced. Unless a reference is provided, all strains were generated in this study.

Non-transgenic strains:

N2, wild type [20]
GR2257, *cth-2(mg599) II* [8]
GR2259, *cth-2(mg599) II; moc-1(ok366) X* [8]
GR2260, *cdo-1(mg622)* [8]
GR2261, *cdo-1(mg622) moc-1(ok366) X* [8]
USD869, *xdh-1(ok3234) IV* (Outcrossed 2X)
USD1033, *sulp-4(rae319) V* (Outcrossed 4X)
USD1037, *sulp-4(rae319) V; cdo-1(mg622) moc-1(ok366) X*
USD1038, *sulp-4(rae319) V; cdo-1(mg622) X*
USD1055, *xdh-1(ok3234) IV; sulp-4(rae334) V*
USD1091, *sulp-4(rae334) V; cdo-1(mg622) X*
USD1103, *cth-2(mg599) II; sulp-4(rae334) V*
USD1105, *cth-2(mg599) II; xdh-1(ok3234) IV; sulp-4(rae334) V*
USD1146, *xdh-1(ok3234) IV; sulp-4(rae334) V; cdo-1(mg622) X*
USD1154, *xdh-1(ok3234) IV; cdo-1(mg622) X*
USD1163, *pnp-1(jy121) IV* (Outcrossed 1X) [23]
USD1170, *cth-2(mg599) II; xdh-1(ok3234) IV*
USD1174, *pnp-1(jy121) xdh-1(ok3234) IV*
USD1198, *pnp-1(jy121) IV; sulp-4(rae319) V*
USD1215, *pnp-1(jy121) xdh-1(ok3234) IV; sulp-4(rae319) V*
USD1269, *exc-5(rh232) xdh-1(ok3234) IV*
USD1308, *osm-8(n1518) II; xdh-1(ok3234) IV*
USD1310, *gpdh-1(ok1558) I* (Outcrossed 4X)
USD1312, *hmit-1.1(ok2923) V* (Outcrossed 4X)
USD1322, *gpdh-1(ok1558) I; sulp-4(rae319) V*
USD1324, *sulp-4(rae319) hmit-1.1(ok2923) V*
USD1327, *osm-8(n1518) II; xdh-1(ok3234) IV; cdo-1(mg622) X*
NJ731, *exc-5(rh232) IV* [26]
MT3571, *osm-8(n1518) II* [34]
RB1082, *sulp-5(ok1048) V*
RB1366, *sulp-2(ok1551) X*
RB1369, *sulp-2(ok1554) X*
RB1436, *sulp-1(ok1639) I*

RB2134, *sulp-8(ok2842) V*

FX08263, *sulp-5(tm8264) X*

VC3021, *sulp-7(ok3751) X*

VC3045, *sulp-7(ok3752) X*

Transgenic strains:

USD1060, *xdh-1(ok3234) IV; sulp-4(rae319) V; raeEx118*

USD1061, *xdh-1(ok3234) IV; sulp-4(rae319) V; raeEx119*

USD1062, *xdh-1(ok3234) IV; sulp-4(rae319) V; raeEx120*

USD1251, *qpIs11 I; sulp-4(rae319) V*

USD1277, *qpIs11 I; exc-5(rh232) IV*

BK36, *qpIs11 I; unc-119(ed3) III* [55]

EMS-derived strains:

USD962*, *xdh-1(ok3234) IV; sulp-4(rae299) V*

USD1007, *xdh-1(ok3234) IV; sulp-4(rae299) V* (Outcrossed 2X)

USD971*, *xdh-1(ok3234) IV; sulp-4(rae302) V*

USD997, *xdh-1(ok3234) IV; sulp-4(rae302) V* (Outcrossed 1X)

USD990*, *xdh-1(ok3234) IV; sulp-4(rae319) V*

USD1001, *xdh-1(ok3234) IV; sulp-4(rae319) V* (Outcrossed 1X)

USD1013*, *xdh-1(ok3234) IV; sulp-4(rae320) V*

USD1019*, *xdh-1(ok3234) IV; sulp-4(rae326) V*

*Whole genome sequencing data for these *C. elegans* strains have been deposited at the NIH Sequence Read Archive (SRA) under accession PRJNA1208078.

CRIPSR/Cas9-derived stains:

USD1042, *sulp-4(rae334) V*

Chemical mutagenesis and whole genome sequencing:

To define *C. elegans* gene activities that were necessary for promoting purine homeostasis, we carried out a chemical mutagenesis screen for mutations that enhanced the penetrance of xanthine stone formation in *xdh-1(ok3234)* mutant *C. elegans* (USD869). *C. elegans* were mutagenized with ethyl methanesulfonate (EMS) using established protocols [20]. F2 generation animals that displayed a xanthine stone were cloned onto individual NGM petri dishes, and F3 generation animals were screened qualitatively for a population-level increase in xanthine stone penetrance. We demanded that new mutant strains of interest were viable and fertile.

Here we report the analysis of 5 new mutant strains (USD962, USD971, USD990, USD1013, and USD1019). Each of these strains carried new EMS-induced lesions (*rae299, rae302, rae319, rae320,* or *rae326)* that enhanced the formation of xanthine stones in an *xdh-1* mutant background. Each mutation was recessive; when heterozygous, each lesion caused 5% (*rae302, n*=42 individuals), 0% (*rae319, n*=38 individuals), 2% (*rae299, n*=41 individuals), or 5% (*rae326, n*=22 individuals) xanthine stone formation in

an *xdh-1* mutant background, dramatically reduced when compared to their homozygous counterparts (**Fig. 2B)**. *rae320* was never characterized as dominant or recessive.

To further genetically analyze these lesions, we performed complementation analyses of these new mutations. The *rae319* lesion failed to complement *rae302* (100% xanthine stone penetrance, *n*=71 individuals), *rae299* (87% xanthine stone penetrance, *n*=38 individuals), and *rae326* (100% xanthine stone penetrance, *n*=14 individuals). All complementation experiments were performed in an *xdh-1(ok3234)* homozygous mutant genetic background. These results suggest *rae302, rae319, rae299,* and *rae326* all impact the same gene. Complementation studies were not performed on *rae320.*

To identify EMS-induced mutations in our strains of interest we followed established protocols [56]. Briefly, whole genomic DNA was prepared from *C. elegans* using the Gentra Puregene Tissue Kit (Qiagen) and genomic DNA libraries were prepared using the NEBNext genomic DNA library construction kit (New England Biolabs). DNA libraries were sequenced on an Illumina NovaSeq and deep sequencing reads were analyzed using standard methods on Galaxy, a web-based platform for computational analyses [57]. Briefly, sequencing reads were trimmed and aligned to the WBcel235 *C. elegans* reference genome [58, 59]. Variations from the reference genome and the putative impact of those variations were annotated and extracted for analysis [60-62]. All 4 strains that formed a complementation group possessed novel mutations in the gene *sulp-4,* strongly suggesting that these lesions in *sulp-4* caused the enhanced xanthine stone formation in the *xdh-1* mutant background (**Fig. 2A, Table S1**). Although the *rae320* lesion found in USD1013 was not analyzed via complementation, whole genome sequence analyses identified a homozygous mutation in *sulp-4*. Thus, we assume that the lesion in *sulp-4* found in USD1013 is also causative for the enhanced xanthine stone formation in the *xdh-1* mutant background (**Table S1)**. In fact, *rae319* and *rae320* are identical genetic lesions. We know that strains carrying these genetic lesions are not siblings as they were derived from independent rounds of mutagenesis. Whole genome sequencing data for these *C. elegans* strains have been deposited at the NIH Sequence Read Archive (SRA) under accession PRJNA1208078.

CRISPR/Cas9 genome editing:

Genome engineering using CRISPR/Cas9 technology was performed using established techniques [21, 22]. Briefly, 2 guide RNAs were designed and synthesized (IDT, crRNA) that targeted the *sulp-4* locus (5’-agagttagctttgtacaacg-3’ and 5’-atagcacatgatacttccgt-3’). Cas9 (IDT) guide RNA ribonucleoprotein complexes were directly injected into the *C. elegans* germline [21]. Newly induced deletions were identified in the offspring of injected animals using a PCR-based screening approach. The DNA primers used to screen for new deletions were: 5’-gcagagaaactcagagcaacaa-3’ and 5’- gcttggtttggaaactttgg-3’. We were able to isolate and homozygoze *sulp-4(rae334),* a new deletion of *sulp-4* (**Fig. 2A**).

C. elegans transgenesis:

Transgenic *C. elegans* carrying extrachromosomal arrays were generated by micro-injecting the gonad of young adult *xdh-1(ok3234); sulp-4(rae319)* double mutant *C. elegans* with an injection mix consisting of the *Psulp-4::SULP-4::GFP* plasmid (20 ng/μl), the *Pmyo-2::mCherry* co-injection marker (2

ng/μl), and the KB+ ladder (78 ng/μl, New England Biolabs) [63]. Three independently derived transgenic strains carrying the extrachromosomal arrays *raeEx118, raeEx119,* or *raeEx120* were isolated and maintained by propagating individual animals based on expression of the fluorescent mCherry protein in the pharynx.

Determination of xanthine stone penetrance:

To determine the percentage of animals that developed a xanthine stone, we cultured wild-type, mutant, and transgenic *C. elegans* beginning at the L4 stage of development under various growth conditions. Animals were assessed daily for the formation of stones and transferred to fresh petri dishes (to avoid contamination from the subsequent generation) over the first 4 days of adulthood except for experiments that used the *cdo-1(mg622)* allele where assays were terminated at day 3 of adulthood. *cdo-1(mg622)* caused early lethality that limited the number of individuals that survived per biological replicate. Thus, the assay was shortened to increase the sample size in **Fig. 1B, 5B, 6B, and S4A**. Importantly, all datapoints in a given figure panel were subjected to the same assay conditions and are thus directly comparable. Xanthine stones were determined based upon presence of exceptionally bright autofluorescent puncta that were opaque when observed by brightfield microscopy. If an individual displayed a stone, it was counted and removed from the assay. If an animal did not display a stone, it was counted and moved to a fresh petri dish to prevent contamination from the subsequent generation and allow for assessment on the following day. Xanthine stone penetrance was the percentage of animals that displayed stone over the course of the assay. If animals went missing or died before the end of the assay, they were not included in the final analyses.

C. elegans larval development and embryonic viability assays:

To assay developmental rates, *C. elegans* were synchronized at the first stage of larval development. To synchronize animals, embryos were harvested from gravid adult animals via treatment with a bleach and sodium hydroxide solution. Embryos were then incubated overnight in M9 solution causing them to hatch and arrest development at the L1 stage [64]. Synchronized L1 animals were cultured for 72 hours, and live animals were imaged as described below. Animal length was measured from tip of head to the end of the tail.

To determine the hatching rate of wild-type and mutant *C. elegans,* we performed synchronized egg lays using young adult animals. Embryos were then scored for hatching ~24 hours after being laid.

Microscopy:

Low magnification bright field and fluorescence images (**Fig. 1C, S1, and S3B-D**) were collected using a Nikon SMZ25 microscope equipped with a Hamamatsu Orca flash 4.0 digital camera using NIS-Elements software (Nikon). High magnification differential interference contrast (DIC) and GFP fluorescence images (**Fig. 2C and 4A,B**) were collected using a Nikon NiE microscope equipped with a Hamamatsu Orca flash 4.0 digital camera using NIS-Elements software (Nikon). All images were processed and analyzed using ImageJ software (NIH). All imaging was performed on live animals paralyzed using sodium azide.

Quantitative PCR (qPCR):

RNA was extracted from synchronized wild-type, *sulp-4(rae319),* and *osm-8(n1518)* young adult animals using Trizol Reagent per manufacturer's instructions (Invitrogen). Prior to RNA extraction, live *C. elegans* samples were washed and subsequently incubated for one hour in buffer M9 to allow for removal of bacterial contamination. cDNA was then synthesized using the GoScript Reverse Transcriptase System following manufacturer's instructions (Promega). qPCR was performed using a CFX96 Real-Time System (Bio-Rad) and SYBR Green Master Mix following manufacturer's instructions (Applied Biosystems). Relative mRNA levels were calculated using the comparative C_T methods [65]. Forward and reverse amplification primers were: *act-1,* 5'-ctcttgccccatcaaccatg-3' and 5'-cttgcttggagatccacatc-3'; *cdo-1,* 5'-ttcgatgagagaaccggaaag-3' and 5'-gccattcttagatcctctgtagtc-3'; *hmit-1.1,* 5'-ccattgaagaggtagaaatgc-3' and 5'-tgtacttcattgtgttgtcc-3'; and *gpdh-1,* 5'-tgcagagattccaggaaaccagg-3' and 5'-ccctttttgtagcttgccacggag-3'.

Acknowledgements:

Some *C. elegans* strains were provided by the CGC, which is funded by the NIH Office of Research Infrastructure Programs (P40 OD010440). We thank the lab of Emily Troemel for providing a *C. elegans* strain carrying the *pnp-1(jy121)* mutation. We thank the lab of Keith Nehrke for providing the *Psulp-4::SULP-4::GFP* plasmid (pTS1). Research reported in this publication was supported by the National Institute of General Medical Sciences of the National Institutes of Health under award number R35 GM146871 (to K.W.). A.V.A. was supported by the National Science Foundation Division of Biological Infrastructure under award number 1756912. C.B. was supported by the National Institute of Childhood Health and Human Development of the National Institutes of Health under award number R25 HD097633.

Figures:

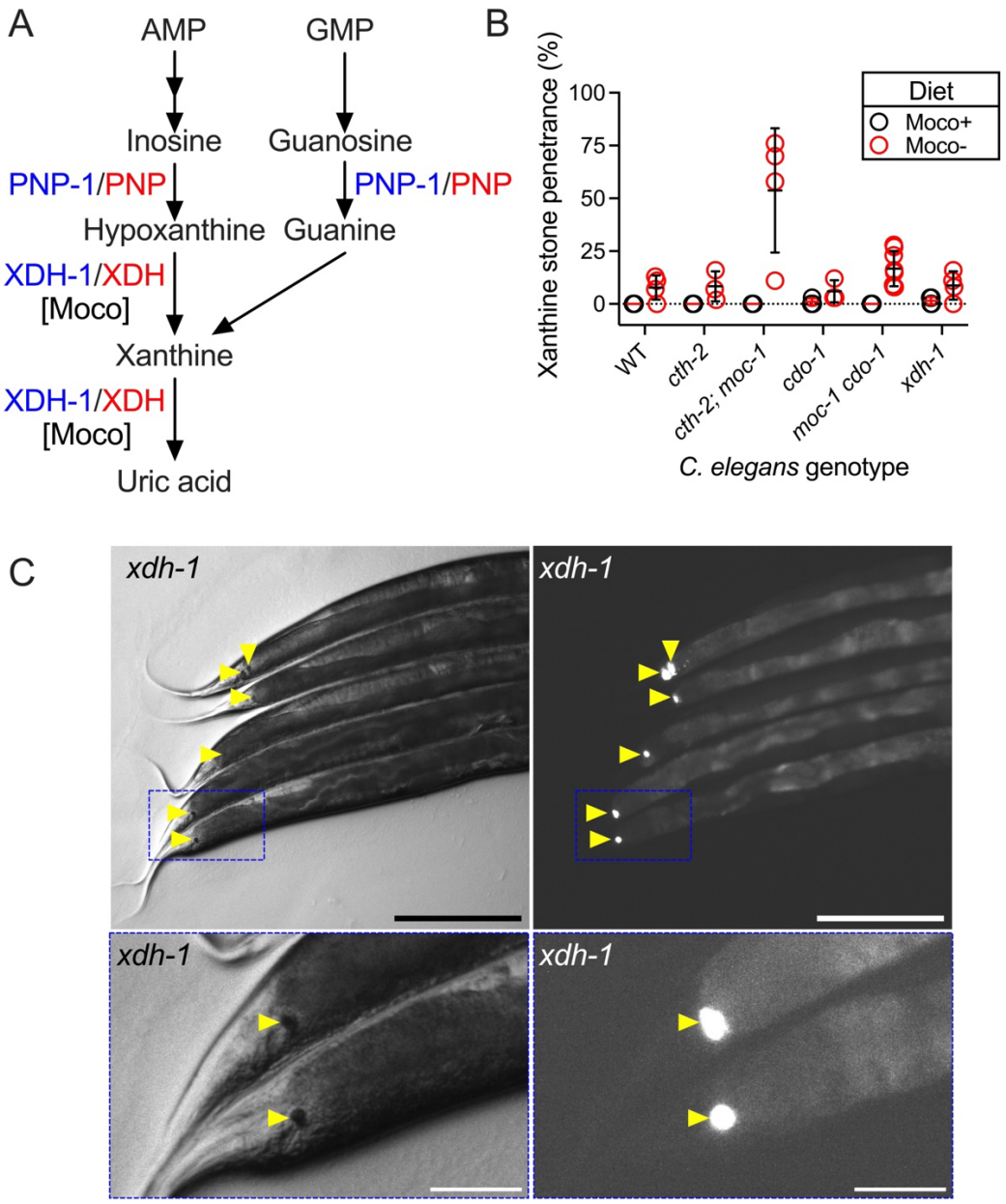

Figure 1: Moco deficiency or loss of *xdh-1* promoted the formation of autofluorescent xanthine stones. A) Purine catabolism pathway. We highlight the roles of purine nucleoside phosphorylase (PNP-1/PNP), and the Moco-requiring enzyme xanthine dehydrogenase (XDH-1/XDH). *C. elegans* enzymes (blue) and their human homologs (red) are displayed. B) Wild-type and mutant *C. elegans* were cultured on wild-type (black, Moco+) or *ΔmoaA* mutant (red, Moco-) *E. coli* and assessed for the formation of xanthine stones over the first 3 days of adulthood. Individual data points represent biological replicates. Mean and standard deviation are displayed. Complete information regarding sample size and individuals scored per biological replicate are found in **Table S2**. C) Brightfield (left) and fluorescent (right) images of the posterior of *xdh-1(ok3234)* mutant adult *C. elegans* cultured on wild-type *E. coli.* Xanthine stones are highlighted (yellow arrowheads). The blue box indicates the region magnified in the lower panels. Scale bar is 250μm (top) or 50μm (bottom).

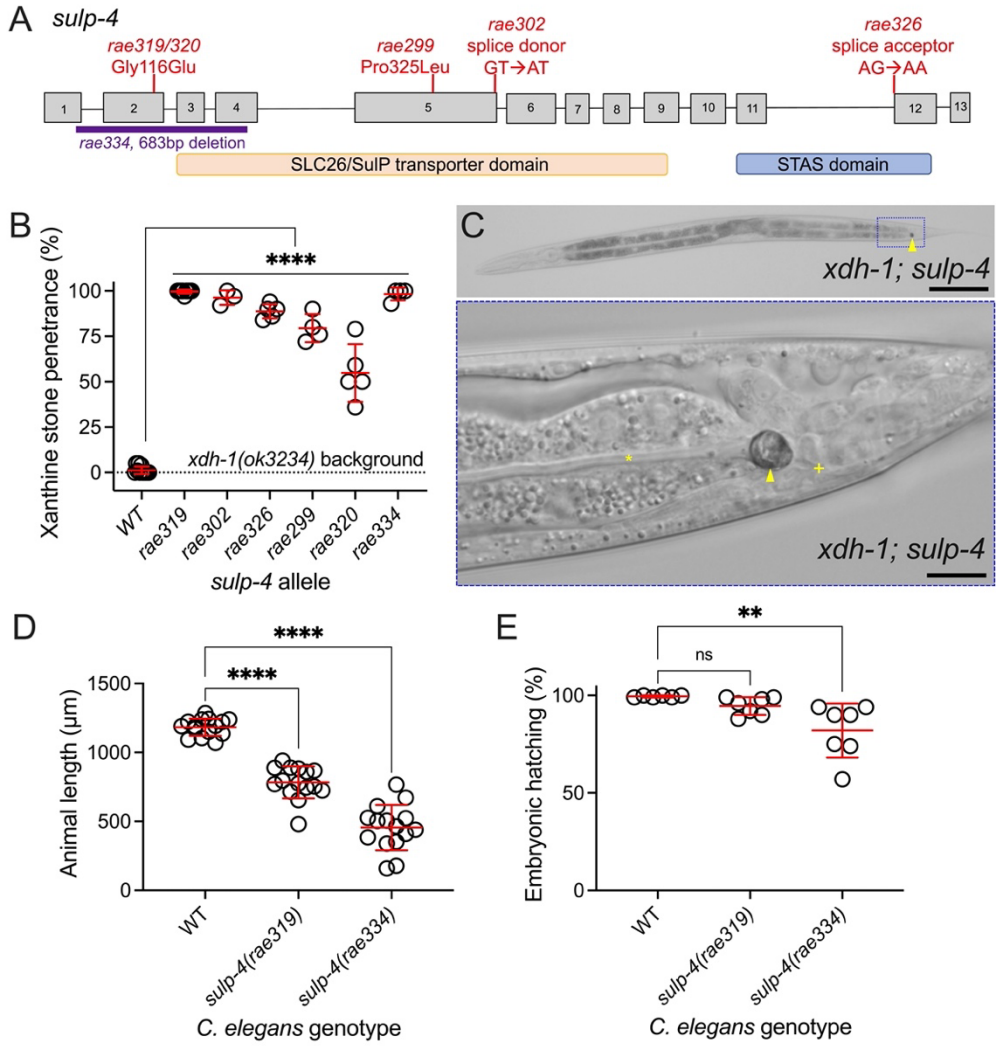

Figure 2: Loss-of-function mutations in *sulp-4* enhanced the formation of xanthine stones during *xdh-1* deficiency. A) *sulp-4* locus. Gray boxes are exons and lines are introns. The regions that encode the SLC26/SulP sulfate permease domain (orange) and STAS domain (blue) are displayed. Red lines display the location of new EMS-induced lesions that enhance the formation of xanthine stones in an *xdh-1(ok3234)* mutant background. *rae334* (purple) is a deletion allele generated using CRISPR/Cas9 technology. B) Xanthine stone formation was assessed for *xdh-1(ok3234)* mutant *C. elegans* with wild-type (WT) or mutant *sulp-4(rae319, rae302, rae326, rae299, rae320,* or *rae334).* ****, p<0.0001, ordinary one-way ANOVA. Individual data points represent biological replicates. Mean and standard deviation are displayed. Complete information regarding sample size and individuals scored per biological replicate are found in **Table S2**. C) Differential interference contrast image of *xdh-1(ok3234); sulp-4(rae319) C. elegans* at the L4 stage of development. Blue box indicates the region magnified in the lower panel. Yellow arrowhead identifies the xanthine stone. Yellow asterisk identifies the lumen of the intestine. Yellow plus sign identifies the rectum. Scale bars are 100µm (top) and 10µm (bottom). D) Wild-type, *sulp-4(rae319),* and *sulp-4(rae334)* mutant *C. elegans* were synchronized at the first stage of larval development and cultured for 72 hours on wild-type *E. coli.* Animal length was determined. Individual datapoints are displayed as are the mean and standard deviation. The sample size is 15 individuals per genotype. ****, p<0.0001, ordinary one-way ANOVA. E) The hatching rate of newly laid wild-type, *sulp-4(rae319),* and *sulp-4(rae334)* mutant *C. elegans* embryos was determined. Individual data points represent biological replicates. Mean and standard deviation are displayed. Complete information regarding sample size and individuals scored per biological replicate are found in **Table S2**. **, p<0.01 or ns, p>0.05, ordinary one-way ANOVA.

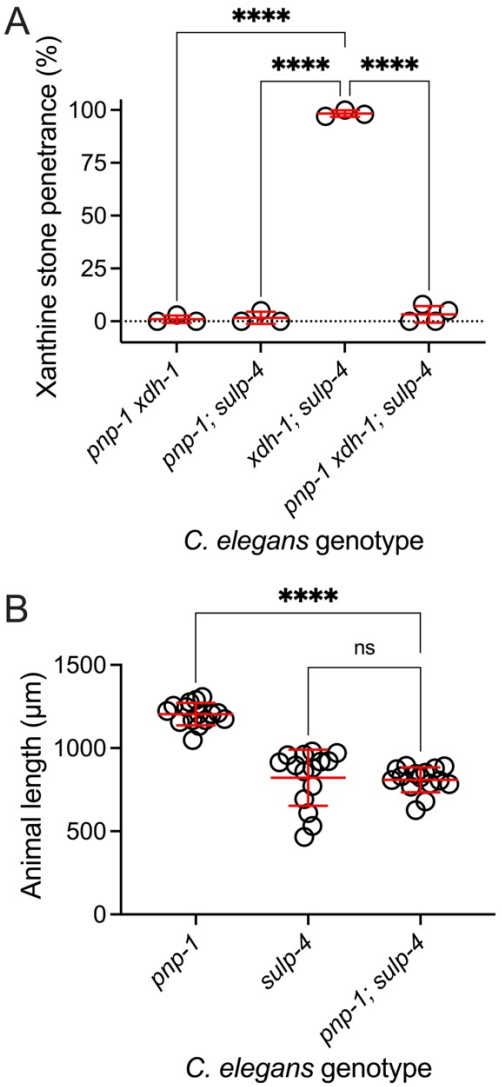

680

681 **Figure 3:** *pnp-1* was required for xanthine stone formation displayed by *xdh-1; sulp-4* mutants but not the
682 larval delay caused by *sulp-4* loss of function.
683 A) Double and triple mutant *C. elegans* were assessed for xanthine stone formation when cultured on wild-
684 type *E. coli*. ****, p<0.0001, ordinary one-way ANOVA. Individual data points represent biological
685 replicates. Mean and standard deviation are displayed. Complete information regarding sample size and
686 individuals scored per biological replicate are found in **Table S2**. B) *pnp-1(jy121), sulp-4(rae319),* and *pnp-*
687 *1(jy121); sulp-4(rae319)* mutant *C. elegans* were synchronized at the first stage of larval development and
688 cultured for 72 hours on wild-type *E. coli.* Animal length was determined. Individual datapoints are
689 displayed as are the mean and standard deviation. The sample size is 15 individuals per genotype. ****,
690 p<0.0001 or ns, p>0.05, ordinary one-way ANOVA.

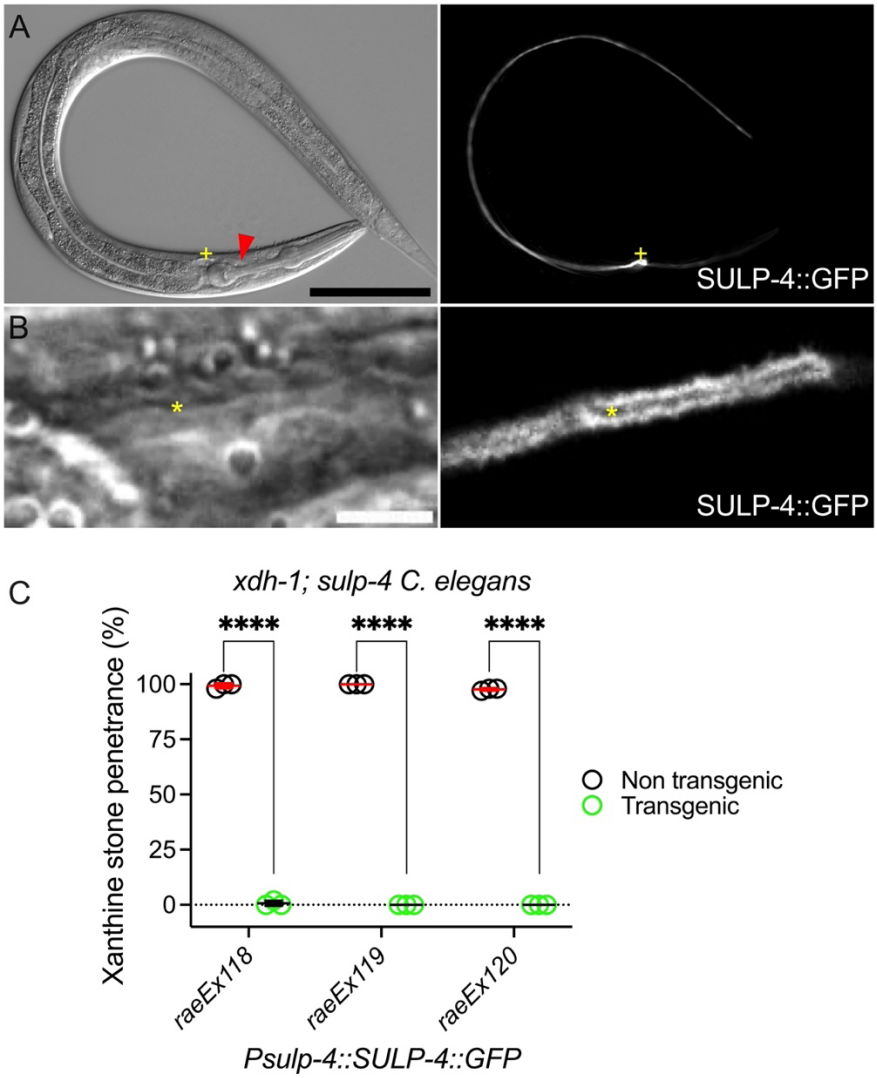

Figure 4: *sulp-4* acted cell non-autonomously in the excretory cell to limit xanthine stone formation. A,B) Differential interference contrast (left) and fluorescence imaging (right) of *xdh-1(ok3234); sulp-4(rae319) C. elegans* expressing the *Psulp-4::SULP-4::GFP* transgene (SULP-4::GFP). Yellow plus sign identifies the cell body of the excretory cell. Red arrow indicates the region magnified in panel B. Yellow asterisk identifies the lumen of the excretory cell. Scale bars are 100μm (A, top) and 5μm (B, bottom). C) Transgenic *xdh-1(ok3234); sulp-4(rae319) C. elegans* expressing the *Psulp-4::SULP-4::GFP* transgene (green) and their non-transgenic siblings (black) were assessed for the formation of xanthine stones. Individual data points represent biological replicates. Mean and standard deviation are displayed. ****, $p<0.0001$, multiple unpaired t tests. Complete information regarding sample size and individuals scored per biological replicate are found in **Table S2**.

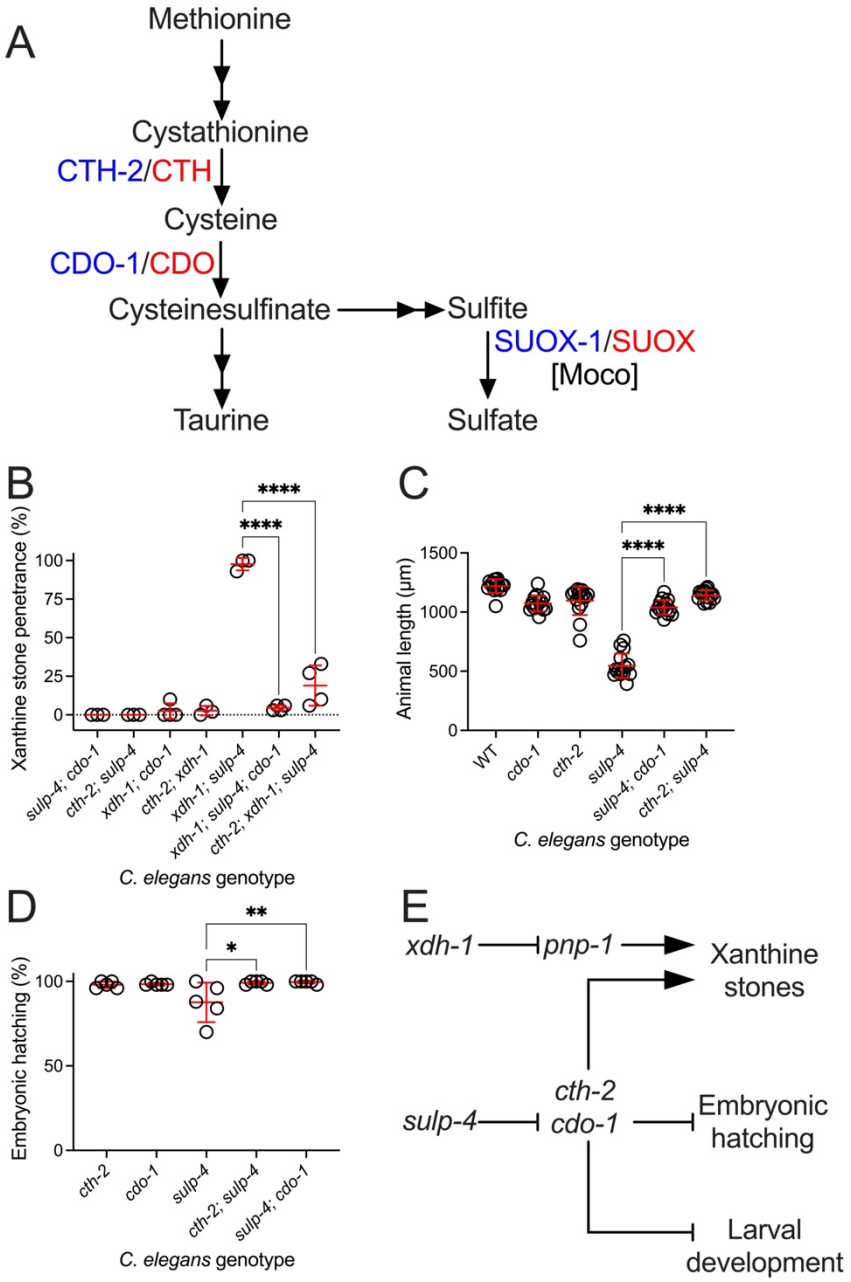

Figure 5: *cth-2* and *cdo-1* were required for phenotypes caused by *sulp-4* loss of function.

A) Sulfur amino acid catabolism pathway. We highlight the roles of cystathionase (CTH-2/CTH), cysteine dioxygenase (CDO-1/CDO), and the Moco-requiring enzyme sulfite oxidase (SUOX-1/SUOX). *C. elegans* enzymes (blue) and their human homologs (red) are displayed. B) Double and triple mutant *C. elegans* were assessed for xanthine stone formation when cultured on wild-type *E. coli* over the first 3 days of adulthood. Individual data points represent biological replicates. Mean and standard deviation are displayed. ****, p<0.0001, ordinary one-way ANOVA. Complete information regarding sample size and individuals scored per biological replicate are found in **Table S2**. C) Wild-type and mutant *C. elegans* were synchronized at the first stage of larval development and cultured for 72 hours on wild type *E. coli.* Animal length was determined. Individual datapoints are displayed as are the mean and standard deviation. The sample size is 15 individuals per genotype. ****, p<0.0001, ordinary one-way ANOVA. D) The hatching rate of newly laid single and double mutant *C. elegans* embryos was determined. Individual data points represent biological replicates. Mean and standard deviation are displayed. **, p<0.01 or *, p<0.05, ordinary one-way ANOVA. Complete information regarding sample size and individuals scored per biological replicate are found in **Table S2**. The *sulp-4(rae334)* allele was used to generate the data in **Fig. 5B-D.** E) A genetic pathway outlining the roles of *xdh-1, pnp-1, sulp-4, cth-2,* and *cdo-1* in governing xanthine stone formation, embryonic hatching, and larval development.

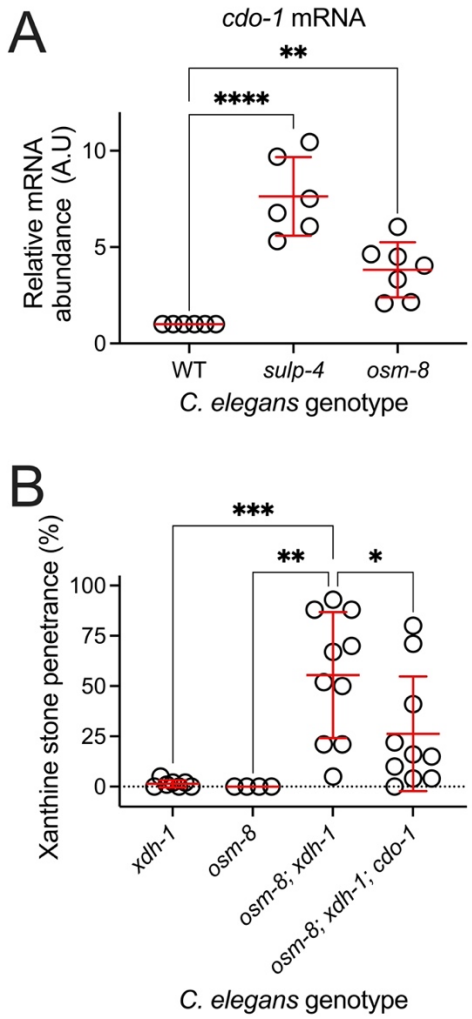

Figure 6: Loss of *osm-8,* which activates the osmotic stress response, enhanced xanthine stone accumulation in *xdh-1* mutant *C. elegans.*

A) Relative mRNA levels of *cdo-1* are displayed for total RNA isolated from wild-type, *sulp-4(rae319)*, and *osm-8(n1518)* young adult *C. elegans.* Relative mRNA abundance was determined via the delta-delta C_T method. All transcripts are normalized to *act-1.* Relative mRNA abundance for each transcript was set to one in the wild type. ****, p<0.0001, **, p<0.01, ordinary one-way ANOVA. B) Mutant *C. elegans* were assessed for xanthine stone formation when cultured on wild-type *E. coli*. Individual data points represent biological replicates. Mean and standard deviation are displayed. ***, p<0.001, **, p<0.01, *, p<0.05, ordinary one-way ANOVA. Complete information regarding sample size and individuals scored per biological replicate are found in **Table S2**.

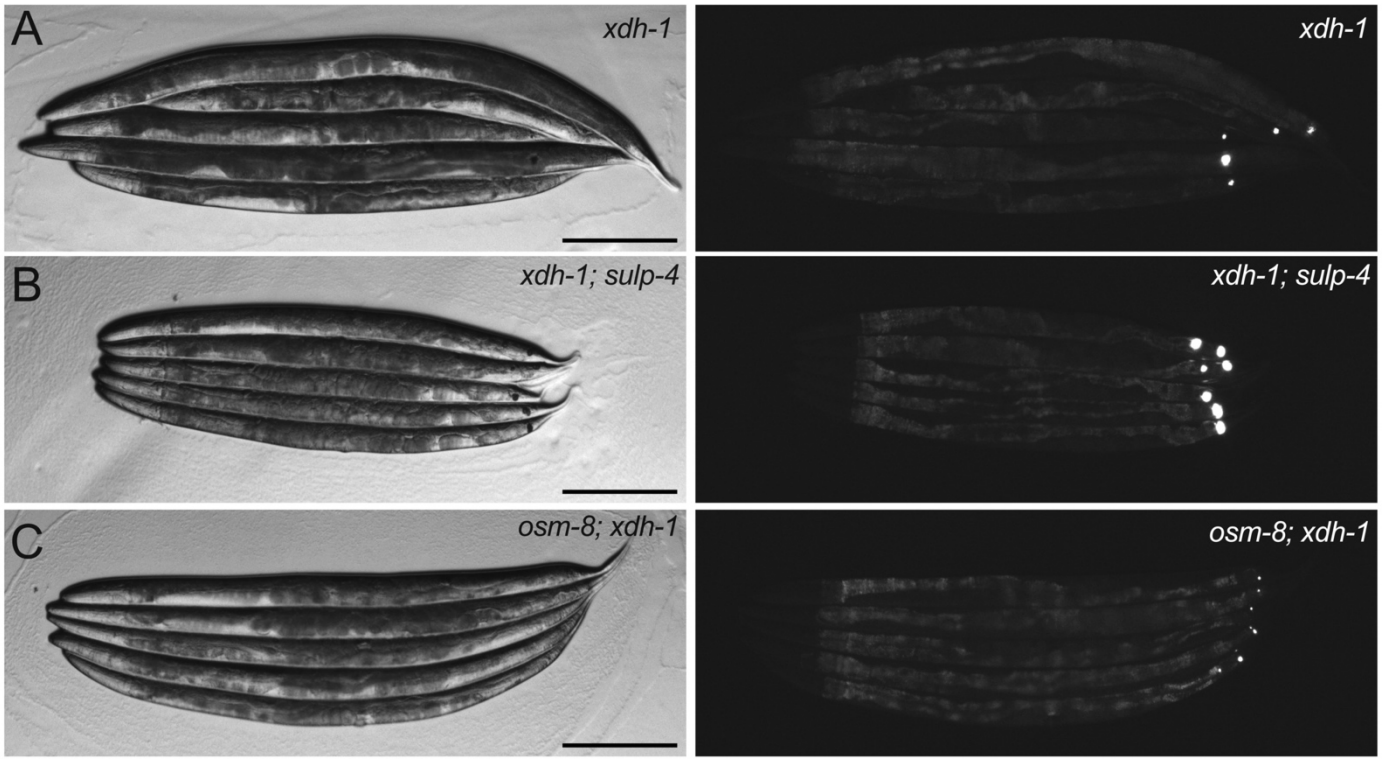

Supplementary Figure 1: Loss of *sulp-4* enhanced the expressivity of the xanthine stone phenotype displayed by *xdh-1* mutant animals.

Brightfield (left) and fluorescent (right) images of the posterior of A) *xdh-1(ok3234)* and B) *xdh-1(ok3234); sulp-4(rae319)* or C) *osm-8(n1518); xdh-1(ok3234)* mutant adult *C. elegans* cultured on wild-type *E. coli.* Scale bar is 250μm. Note, *xdh-1(ok3234)* animals displayed are older than their *xdh-1(ok3234); sulp-4(rae319)* or *osm-8(n1518); xdh-1(ok3234)* counterparts which were imaged as day 2 adults. This was necessary to allow us to identify sufficient *xdh-1* single mutant animals displaying a xanthine stone.

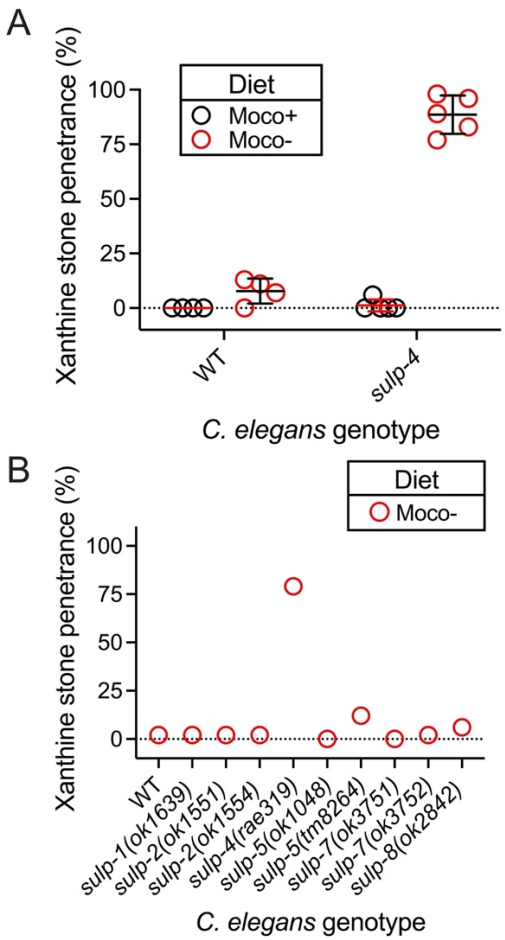

Supplementary Figure 2: Inactivating mutations in *sulp* genes other than *sulp-4* did not enhance xanthine stone formation during dietary Moco deficiency.

A) Wild-type and *sulp-4(rae319) C. elegans* were cultured on wild-type (black, Moco+) or *ΔmoaA* mutant (red, Moco-) *E. coli* and assessed for the formation of xanthine stones. Note, data points for the wild-type animals cultured on Moco+ and Moco- *E. coli* are derived from the same experiment that is displayed in Figure 1B. However, in this analysis the animals were scored until day 4 of adulthood. B) Wild type and viable *sulp* mutant *C. elegans* were cultured on *ΔmoaA* mutant (red, Moco-) *E. coli* and assessed for the formation of xanthine stones. Data points represent a single biological replicate with 19-53 individuals per replicate. Complete information regarding individuals scored per biological replicate are found in **Table S2**.

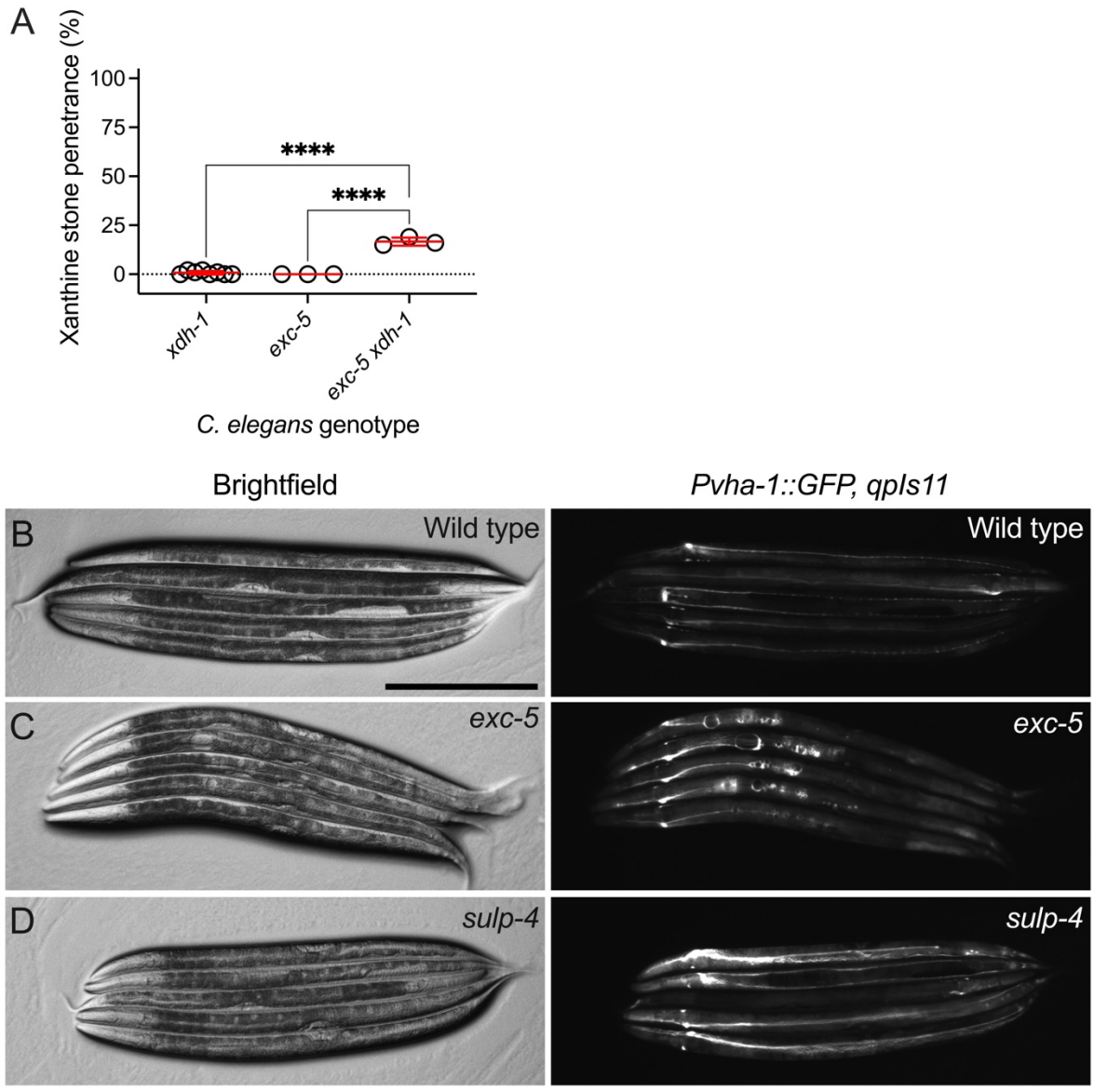

Supplementary Figure 3: Loss of *exc-5* modestly enhanced the formation of xanthine stones in an *xdh-1* mutant background while *sulp-4* loss of function does not impact excretory cell morphology.

A) *xdh-1(ok3234), exc-5(rh232),* and *exc-5(rh232) xdh-1(ok3234)* mutant *C. elegans* were assessed for xanthine stone formation when cultured on wild-type *E. coli*. Individual data points represent biological replicates. Mean and standard deviation are displayed. ****, p<0.0001, ordinary one-way ANOVA. Complete information regarding sample size and individuals scored per biological replicate are found in **Table S2**. B-D) Brightfield (left) and fluorescence imaging (right) are displayed for B) wild-type, C) *exc-5(rh232),* or D) *sulp-4(rae319) C. elegans* expressing the *qpIs11* (*Pvha-1::GFP)* transgene, which marks the excretory cell. Scale bar is 250μm

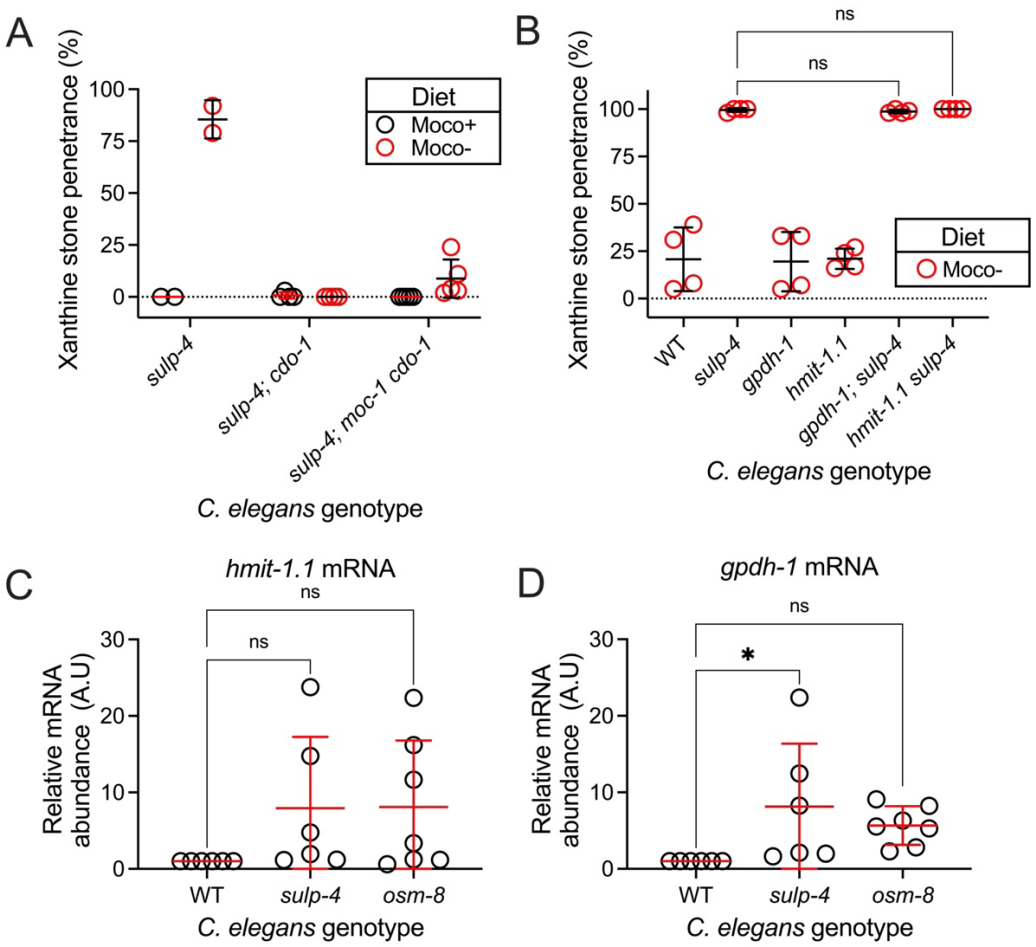

Supplementary Figure 4: *cdo-1,* but not *hmit-1.1* or *gpdh-1,* was necessary for the enhanced formation of xanthine stones caused by *sulp-4* inactivation during dietary Moco deficiency.

A) *sulp-4(rae319), sulp-4(rae319); cdo-1(mg622),* and *sulp-4(rae319); moc-1(ok366) cdo-1(mg622)* mutant *C. elegans* were cultured on wild-type (black, Moco+) or *ΔmoaA* mutant (red, Moco-) *E. coli* and assessed for the formation of xanthine stones over the first 3 days of adulthood. B) Wild type and mutant *C. elegans* were cultured on *ΔmoaA* mutant (red, Moco-) *E. coli* and assessed for the formation of xanthine stones. Individual data points represent biological replicates. Mean and standard deviation are displayed. ns, p>0.05, ordinary one-way ANOVA. Complete information regarding sample size and individuals scored per biological replicate are found in **Table S2**. Relative mRNA expression of C) *hmit-1.1* and D) *gpdh-1* are displayed for total RNA isolated from wild-type, *sulp-4(rae319)*, and *osm-8(n1518)* young adult *C. elegans.* Relative mRNA abundance was determined via the delta-delta C_T method. All transcripts are normalized to *act-1.* Relative mRNA abundance for each transcript was set to one in the wild type. *, p<0.05, ns, p>0.05, ordinary one-way ANOVA.

Strain	Allele	Chromosome	Chromosome position	Gene affected	Reference base	Mutant base	Allele status	Variant impact
USD962	*rae299*	V	11876913	*sulp-4*	C	T	Homozygous	Pro325Leu
USD971	*rae302*	V	11877161	*sulp-4*	G	A	Homozygous	Splice donor variant
USD990	*rae319*	V	11875799	*sulp-4*	G	A	Homozygous	Gly116Glu
USD1013	*rae320*	V	11875799	*sulp-4*	G	A	Homozygous	Gly116Glu
USD1019	*rae326*	V	11878726	*sulp-4*	G	A	Homozygous	Splice acceptor variant

Supplementary Table 1: EMS-induced lesions in *sulp-4* that promoted the formation of xanthine stones in *xdh-1(ok3234)*-mutant *C. elegans.*

Supplementary Table 2: Raw data and information regarding sample sizes and biological replicates.

Literature cited:

1. Mullen NJ, Singh PK. Nucleotide metabolism: a pan-cancer metabolic dependency. Nat Rev Cancer. 2023;23(5):275-94. Epub 2023/03/28. doi: 10.1038/s41568-023-00557-7. PubMed PMID: 36973407; PubMed Central PMCID: PMCPMC10041518.
2. Lesch M, Nyhan WL. A FAMILIAL DISORDER OF URIC ACID METABOLISM AND CENTRAL NERVOUS SYSTEM FUNCTION. Am J Med. 1964;36:561-70. Epub 1964/04/01. doi: 10.1016/0002-9343(64)90104-4. PubMed PMID: 14142409.
3. Giblett ER, Ammann AJ, Wara DW, Sandman R, Diamond LK. Nucleoside-phosphorylase deficiency in a child with severely defective T-cell immunity and normal B-cell immunity. Lancet. 1975;1(7914):1010-3. Epub 1975/05/03. doi: 10.1016/s0140-6736(75)91950-9. PubMed PMID: 48676.
4. Duran M, Beemer FA, van de Heiden C, Korteland J, de Bree PK, Brink M, et al. Combined deficiency of xanthine oxidase and sulphite oxidase: a defect of molybdenum metabolism or transport? J Inherit Metab Dis. 1978;1(4):175-8. Epub 1978/01/01. doi: 10.1007/bf01805591. PubMed PMID: 117254.
5. Dent CE, Philpot GR. Xanthinuria, an inborn error (or deviation) of metabolism. Lancet. 1954;266(6804):182-5. Epub 1954/01/23. doi: 10.1016/s0140-6736(54)91257-x. PubMed PMID: 13118765.
6. Ball EG. XANTHINE OXIDASE: PURIFICATION AND PROPERTIES. J Biol Chem. 1939;128(1):51-67.
7. Sebesta I. Genetic disorders resulting in hyper- or hypouricemia. Adv Chronic Kidney Dis. 2012;19(6):398-403. Epub 2012/10/24. doi: 10.1053/j.ackd.2012.06.002. PubMed PMID: 23089275.
8. Warnhoff K, Ruvkun G. Molybdenum cofactor transfer from bacteria to nematode mediates sulfite detoxification. Nat Chem Biol. 2019;15(5):480-8. Epub 2019/03/27. doi: 10.1038/s41589-019-0249-y. PubMed PMID: 30911177; PubMed Central PMCID: PMCPMC6470025.
9. Schwarz G, Mendel RR, Ribbe MW. Molybdenum cofactors, enzymes and pathways. Nature. 2009;460(7257):839-47. Epub 2009/08/14. doi: 10.1038/nature08302. PubMed PMID: 19675644.
10. Snoozy J, Breen PC, Ruvkun G, Warnhoff K. moc-6/MOCS2A is necessary for molybdenum cofactor synthesis in C. elegans. MicroPubl Biol. 2022;2022. Epub 2022/03/01. doi: 10.17912/micropub.biology.000531. PubMed PMID: 35224462; PubMed Central PMCID: PMCPMC8864482.
11. Warnhoff K, Hercher TW, Mendel RR, Ruvkun G. Protein-bound molybdenum cofactor is bioavailable and rescues molybdenum cofactor-deficient C. elegans. Genes Dev. 2021;35(3-

4):212-7. Epub 2021/01/16. doi: 10.1101/gad.345579.120. PubMed PMID: 33446569; PubMed Central PMCID: PMCPMC7849362.

12. Oliphant KD, Fettig RR, Snoozy J, Mendel RR, Warnhoff K. Obtaining the necessary molybdenum cofactor for sulfite oxidase activity in the nematode Caenorhabditis elegans surprisingly involves a dietary source. J Biol Chem. 2023;299(1):102736. Epub 2022/11/25. doi: 10.1016/j.jbc.2022.102736. PubMed PMID: 36423681; PubMed Central PMCID: PMCPMC9793310.

13. Sherman T, Chernova MN, Clark JS, Jiang L, Alper SL, Nehrke K. The abts and sulp families of anion transporters from Caenorhabditis elegans. Am J Physiol Cell Physiol. 2005;289(2):C341-51. Epub 2005/04/09. doi: 10.1152/ajpcell.00071.2005. PubMed PMID: 15814591.

14. Nelson FK, Riddle DL. Functional study of the Caenorhabditis elegans secretory-excretory system using laser microsurgery. J Exp Zool. 1984;231(1):45-56. Epub 1984/07/01. doi: 10.1002/jez.1402310107. PubMed PMID: 6470649.

15. Chalmers RA, Watts RW, Pallis C, Bitensky L, Chayen J. Crystalline deposits in striped muscle in xanthinuria. Nature. 1969;221(5176):170-1. Epub 1969/01/11. doi: 10.1038/221170a0. PubMed PMID: 5782709.

16. Watts RW, Engelman K, Klinenberg JR, Seegmiller JE, Sjoerdsma A. ENZYME DEFECT IN A CASE OF XANTHINURIA. Nature. 1964;201:395-6. Epub 1964/01/25. doi: 10.1038/201395a0. PubMed PMID: 14110004.

17. Ma X, Wang W, Bittner F, Schmidt N, Berkey R, Zhang L, et al. Dual and Opposing Roles of Xanthine Dehydrogenase in Defense-Associated Reactive Oxygen Species Metabolism in Arabidopsis. Plant Cell. 2016;28(5):1108-26. Epub 2016/05/07. doi: 10.1105/tpc.15.00880. PubMed PMID: 27152019; PubMed Central PMCID: PMCPMC4904670.

18. Chi T, Kim MS, Lang S, Bose N, Kahn A, Flechner L, et al. A Drosophila model identifies a critical role for zinc in mineralization for kidney stone disease. PLoS One. 2015;10(5):e0124150. Epub 2015/05/15. doi: 10.1371/journal.pone.0124150. PubMed PMID: 25970330; PubMed Central PMCID: PMCPMC4430225.

19. Glassman E, Mitchell HK. Mutants of Drosophila Melanogaster Deficient in Xanthine Dehydrogenase. Genetics. 1959;44(2):153-62. Epub 1959/03/01. doi: 10.1093/genetics/44.2.153. PubMed PMID: 17247815; PubMed Central PMCID: PMCPMC1209939.

20. Brenner S. The genetics of Caenorhabditis elegans. Genetics. 1974;77(1):71-94. Epub 1974/05/01. PubMed PMID: 4366476; PubMed Central PMCID: PMCPMC1213120.

21. Cho SW, Lee J, Carroll D, Kim JS, Lee J. Heritable gene knockout in Caenorhabditis elegans by direct injection of Cas9-sgRNA ribonucleoproteins. Genetics. 2013;195(3):1177-80. Epub 2013/08/28. doi: 10.1534/genetics.113.155853. PubMed PMID: 23979576; PubMed Central PMCID: PMCPMC3813847.

22. Ghanta KS, Mello CC. Melting dsDNA Donor Molecules Greatly Improves Precision Genome Editing in Caenorhabditis elegans. Genetics. 2020;216(3):643-50. Epub 2020/09/24. doi: 10.1534/genetics.120.303564. PubMed PMID: 32963112; PubMed Central PMCID: PMCPMC7648581.

23. Tecle E, Chhan CB, Franklin L, Underwood RS, Hanna-Rose W, Troemel ER. The purine nucleoside phosphorylase pnp-1 regulates epithelial cell resistance to infection in C. elegans. PLoS Pathog. 2021;17(4):e1009350. Epub 2021/04/21. doi: 10.1371/journal.ppat.1009350. PubMed PMID: 33878133; PubMed Central PMCID: PMCPMC8087013.

24. Altschul SF, Gish W, Miller W, Myers EW, Lipman DJ. Basic local alignment search tool. J Mol Biol. 1990;215(3):403-10. Epub 1990/10/05. doi: 10.1016/s0022-2836(05)80360-2. PubMed PMID: 2231712.

25. Buechner M. Tubes and the single C. elegans excretory cell. Trends Cell Biol. 2002;12(10):479-84. Epub 2002/11/21. doi: 10.1016/s0962-8924(02)02364-4. PubMed PMID: 12441252.

26. Suzuki N, Buechner M, Nishiwaki K, Hall DH, Nakanishi H, Takai Y, et al. A putative GDP-GTP exchange factor is required for development of the excretory cell in Caenorhabditis elegans. EMBO Rep. 2001;2(6):530-5. Epub 2001/06/21. doi: 10.1093/embo-reports/kve110. PubMed PMID: 11415987; PubMed Central PMCID: PMCPMC1083904.
27. Warnhoff K, Bhattacharya S, Snoozy J, Breen PC, Ruvkun G. Hypoxia-inducible factor induces cysteine dioxygenase and promotes cysteine homeostasis in Caenorhabditis elegans. Elife. 2024;12. Epub 2024/02/13. doi: 10.7554/eLife.89173. PubMed PMID: 38349720.
28. Stipanuk MH, Ueki I. Dealing with methionine/homocysteine sulfur: cysteine metabolism to taurine and inorganic sulfur. J Inherit Metab Dis. 2011;34(1):17-32. Epub 2010/02/18. doi: 10.1007/s10545-009-9006-9. PubMed PMID: 20162368; PubMed Central PMCID: PMCPMC2901774.
29. Lee SD, Choi SY, Lim SW, Lamitina ST, Ho SN, Go WY, et al. TonEBP stimulates multiple cellular pathways for adaptation to hypertonic stress: organic osmolyte-dependent and -independent pathways. Am J Physiol Renal Physiol. 2011;300(3):F707-15. Epub 2011/01/07. doi: 10.1152/ajprenal.00227.2010. PubMed PMID: 21209002; PubMed Central PMCID: PMCPMC3064130.
30. Lamitina T, Huang CG, Strange K. Genome-wide RNAi screening identifies protein damage as a regulator of osmoprotective gene expression. Proc Natl Acad Sci U S A. 2006;103(32):12173-8. Epub 2006/08/02. doi: 10.1073/pnas.0602987103. PubMed PMID: 16880390; PubMed Central PMCID: PMCPMC1567714.
31. Lamitina ST, Morrison R, Moeckel GW, Strange K. Adaptation of the nematode Caenorhabditis elegans to extreme osmotic stress. Am J Physiol Cell Physiol. 2004;286(4):C785-91. Epub 2003/12/03. doi: 10.1152/ajpcell.00381.2003. PubMed PMID: 14644776.
32. Kage-Nakadai E, Uehara T, Mitani S. H+/myo-inositol transporter genes, hmit-1.1 and hmit-1.2, have roles in the osmoprotective response in Caenorhabditis elegans. Biochem Biophys Res Commun. 2011;410(3):471-7. Epub 2011/06/18. doi: 10.1016/j.bbrc.2011.06.001. PubMed PMID: 21679696.
33. Rohlfing AK, Miteva Y, Hannenhalli S, Lamitina T. Genetic and physiological activation of osmosensitive gene expression mimics transcriptional signatures of pathogen infection in C. elegans. PLoS One. 2010;5(2):e9010. Epub 2010/02/04. doi: 10.1371/journal.pone.0009010. PubMed PMID: 20126308; PubMed Central PMCID: PMCPMC2814864.
34. Rohlfing AK, Miteva Y, Moronetti L, He L, Lamitina T. The Caenorhabditis elegans mucin-like protein OSM-8 negatively regulates osmosensitive physiology via the transmembrane protein PTR-23. PLoS Genet. 2011;7(1):e1001267. Epub 2011/01/22. doi: 10.1371/journal.pgen.1001267. PubMed PMID: 21253570; PubMed Central PMCID: PMCPMC3017116.
35. Yanagi KS, Jochim B, Kunjo SO, Breen P, Ruvkun G, Lehrbach N. Mutations in nucleotide metabolism genes bypass proteasome defects in png-1/NGLY1-deficient Caenorhabditis elegans. PLoS Biol. 2024;22(7):e3002720. Epub 2024/07/11. doi: 10.1371/journal.pbio.3002720. PubMed PMID: 38991033; PubMed Central PMCID: PMCPMC11265709.
36. Ast T, Meisel JD, Patra S, Wang H, Grange RMH, Kim SH, et al. Hypoxia Rescues Frataxin Loss by Restoring Iron Sulfur Cluster Biogenesis. Cell. 2019;177(6):1507-21.e16. Epub 2019/04/30. doi: 10.1016/j.cell.2019.03.045. PubMed PMID: 31031004; PubMed Central PMCID: PMCPMC6911770.
37. Bantia S, Parker C, Upshaw R, Cunningham A, Kotian P, Kilpatrick JM, et al. Potent orally bioavailable purine nucleoside phosphorylase inhibitor BCX-4208 induces apoptosis in B- and T-lymphocytes--a novel treatment approach for autoimmune diseases, organ transplantation and hematologic malignancies. Int Immunopharmacol. 2010;10(7):784-90. Epub 2010/04/20. doi: 10.1016/j.intimp.2010.04.009. PubMed PMID: 20399911.

38. Kamath VP, Juarez-Brambila JJ, Morris PE, Jr. Synthesis of labeled BCX-4208, a potent inhibitor of purine nucleoside phosphorylase. Drug Test Anal. 2009;1(3):125-7. Epub 2010/04/01. doi: 10.1002/dta.24. PubMed PMID: 20355185.
39. Dorwart MR, Shcheynikov N, Yang D, Muallem S. The solute carrier 26 family of proteins in epithelial ion transport. Physiology (Bethesda). 2008;23:104-14. Epub 2008/04/11. doi: 10.1152/physiol.00037.2007. PubMed PMID: 18400693.
40. Sindić A, Chang MH, Mount DB, Romero MF. Renal physiology of SLC26 anion exchangers. Curr Opin Nephrol Hypertens. 2007;16(5):484-90. Epub 2007/08/19. doi: 10.1097/MNH.0b013e3282e7d7d0. PubMed PMID: 17693766.
41. Hill AJ, Basourakos SP, Lewicki P, Wu X, Arenas-Gallo C, Chuang D, et al. Incidence of Kidney Stones in the United States: The Continuous National Health and Nutrition Examination Survey. J Urol. 2022;207(4):851-6. Epub 2021/12/03. doi: 10.1097/ju.0000000000002331. PubMed PMID: 34854755.
42. Moe OW. Kidney stones: pathophysiology and medical management. Lancet. 2006;367(9507):333-44. Epub 2006/01/31. doi: 10.1016/s0140-6736(06)68071-9. PubMed PMID: 16443041.
43. Jiang Z, Asplin JR, Evan AP, Rajendran VM, Velazquez H, Nottoli TP, et al. Calcium oxalate urolithiasis in mice lacking anion transporter Slc26a6. Nat Genet. 2006;38(4):474-8. Epub 2006/03/15. doi: 10.1038/ng1762. PubMed PMID: 16532010.
44. Cornière N, Thomson RB, Thauvin S, Villoutreix BO, Karp S, Dynia DW, et al. Dominant negative mutation in oxalate transporter SLC26A6 associated with enteric hyperoxaluria and nephrolithiasis. J Med Genet. 2022;59(11):1035-43. Epub 2022/02/05. doi: 10.1136/jmedgenet-2021-108256. PubMed PMID: 35115415; PubMed Central PMCID: PMCPMC9346097.
45. Gee HY, Jun I, Braun DA, Lawson JA, Halbritter J, Shril S, et al. Mutations in SLC26A1 Cause Nephrolithiasis. Am J Hum Genet. 2016;98(6):1228-34. Epub 2016/05/24. doi: 10.1016/j.ajhg.2016.03.026. PubMed PMID: 27210743; PubMed Central PMCID: PMCPMC4908148.
46. Hirata T, Cabrero P, Berkholz DS, Bondeson DP, Ritman EL, Thompson JR, et al. In vivo Drosophilia genetic model for calcium oxalate nephrolithiasis. Am J Physiol Renal Physiol. 2012;303(11):F1555-62. Epub 2012/09/21. doi: 10.1152/ajprenal.00074.2012. PubMed PMID: 22993075; PubMed Central PMCID: PMCPMC3532482.
47. Prince CL, Scardino PL, Wolan CT. The effect of temperature, humidity and dehydration on the formation of renal calculi. J Urol. 1956;75(2):209-15. Epub 1956/02/01. doi: 10.1016/s0022-5347(17)66798-3. PubMed PMID: 13296117.
48. Mudd SH, Irreverre F, Laster L. Sulfite oxidase deficiency in man: demonstration of the enzymatic defect. Science. 1967;156(3782):1599-602. Epub 1967/06/23. doi: 10.1126/science.156.3782.1599. PubMed PMID: 6025118.
49. Dominy JE, Jr., Hirschberger LL, Coloso RM, Stipanuk MH. In vivo regulation of cysteine dioxygenase via the ubiquitin-26S proteasome system. Adv Exp Med Biol. 2006;583:37-47. Epub 2006/12/13. doi: 10.1007/978-0-387-33504-9_4. PubMed PMID: 17153587.
50. Dominy JE, Jr., Hirschberger LL, Coloso RM, Stipanuk MH. Regulation of cysteine dioxygenase degradation is mediated by intracellular cysteine levels and the ubiquitin-26 S proteasome system in the living rat. Biochem J. 2006;394(Pt 1):267-73. Epub 2005/11/03. doi: 10.1042/bj20051510. PubMed PMID: 16262602; PubMed Central PMCID: PMCPMC1386025.
51. Stipanuk MH, Hirschberger LL, Londono MP, Cresenzi CL, Yu AF. The ubiquitin-proteasome system is responsible for cysteine-responsive regulation of cysteine dioxygenase concentration in liver. Am J Physiol Endocrinol Metab. 2004;286(3):E439-48. Epub 2003/12/03. doi: 10.1152/ajpendo.00336.2003. PubMed PMID: 14644768.
52. Lee JI, Londono M, Hirschberger LL, Stipanuk MH. Regulation of cysteine dioxygenase and gamma-glutamylcysteine synthetase is associated with hepatic cysteine level. J Nutr

Biochem. 2004;15(2):112-22. Epub 2004/02/20. doi: 10.1016/j.jnutbio.2003.10.005. PubMed PMID: 14972351.

53. Kwon YH, Stipanuk MH. Cysteine regulates expression of cysteine dioxygenase and gamma-glutamylcysteine synthetase in cultured rat hepatocytes. Am J Physiol Endocrinol Metab. 2001;280(5):E804-15. Epub 2001/04/05. doi: 10.1152/ajpendo.2001.280.5.E804. PubMed PMID: 11287364.

54. Baba T, Ara T, Hasegawa M, Takai Y, Okumura Y, Baba M, et al. Construction of Escherichia coli K-12 in-frame, single-gene knockout mutants: the Keio collection. Mol Syst Biol. 2006;2:2006.0008. Epub 2006/06/02. doi: 10.1038/msb4100050. PubMed PMID: 16738554; PubMed Central PMCID: PMCPMC1681482.

55. Mattingly BC, Buechner M. The FGD homologue EXC-5 regulates apical trafficking in C. elegans tubules. Dev Biol. 2011;359(1):59-72. Epub 2011/09/06. doi: 10.1016/j.ydbio.2011.08.011. PubMed PMID: 21889936; PubMed Central PMCID: PMCPMC3212395.

56. Lehrbach NJ, Ji F, Sadreyev R. Next-Generation Sequencing for Identification of EMS-Induced Mutations in Caenorhabditis elegans. Curr Protoc Mol Biol. 2017;117:7.29.1-7..12. Epub 2017/01/07. doi: 10.1002/cpmb.27. PubMed PMID: 28060408; PubMed Central PMCID: PMCPMC5303615.

57. Community G. The Galaxy platform for accessible, reproducible and collaborative biomedical analyses: 2022 update. Nucleic Acids Res. 2022;50(W1):W345-51. Epub 2022/04/22. doi: 10.1093/nar/gkac247. PubMed PMID: 35446428; PubMed Central PMCID: PMCPMC9252830.

58. Bolger AM, Lohse M, Usadel B. Trimmomatic: a flexible trimmer for Illumina sequence data. Bioinformatics. 2014;30(15):2114-20. Epub 2014/04/04. doi: 10.1093/bioinformatics/btu170. PubMed PMID: 24695404; PubMed Central PMCID: PMCPMC4103590.

59. Li H, Durbin R. Fast and accurate long-read alignment with Burrows-Wheeler transform. Bioinformatics. 2010;26(5):589-95. Epub 2010/01/19. doi: 10.1093/bioinformatics/btp698. PubMed PMID: 20080505; PubMed Central PMCID: PMCPMC2828108.

60. Wilm A, Aw PP, Bertrand D, Yeo GH, Ong SH, Wong CH, et al. LoFreq: a sequence-quality aware, ultra-sensitive variant caller for uncovering cell-population heterogeneity from high-throughput sequencing datasets. Nucleic Acids Res. 2012;40(22):11189-201. Epub 2012/10/16. doi: 10.1093/nar/gks918. PubMed PMID: 23066108; PubMed Central PMCID: PMCPMC3526318.

61. Cingolani P, Patel VM, Coon M, Nguyen T, Land SJ, Ruden DM, et al. Using Drosophila melanogaster as a Model for Genotoxic Chemical Mutational Studies with a New Program, SnpSift. Front Genet. 2012;3:35. Epub 2012/03/22. doi: 10.3389/fgene.2012.00035. PubMed PMID: 22435069; PubMed Central PMCID: PMCPMC3304048.

62. Cingolani P, Platts A, Wang le L, Coon M, Nguyen T, Wang L, et al. A program for annotating and predicting the effects of single nucleotide polymorphisms, SnpEff: SNPs in the genome of Drosophila melanogaster strain w1118; iso-2; iso-3. Fly (Austin). 2012;6(2):80-92. Epub 2012/06/26. doi: 10.4161/fly.19695. PubMed PMID: 22728672; PubMed Central PMCID: PMCPMC3679285.

63. Mello CC, Kramer JM, Stinchcomb D, Ambros V. Efficient gene transfer in C.elegans: extrachromosomal maintenance and integration of transforming sequences. Embo j. 1991;10(12):3959-70. Epub 1991/12/01. doi: 10.1002/j.1460-2075.1991.tb04966.x. PubMed PMID: 1935914; PubMed Central PMCID: PMCPMC453137.

64. Stiernagle T. Maintenance of C. elegans. WormBook. 2006:1-11. Epub 2007/12/01. doi: 10.1895/wormbook.1.101.1. PubMed PMID: 18050451; PubMed Central PMCID: PMCPMC4781397.

1030 65. Schmittgen TD, Livak KJ. Analyzing real-time PCR data by the comparative C(T) method.
1031 Nat Protoc. 2008;3(6):1101-8. Epub 2008/06/13. doi: 10.1038/nprot.2008.73. PubMed PMID:
1032 18546601.
1033